Applied Catalysis B: Environmental 233 (2018) 301–317

Contents lists available at ScienceDirect

Applied Catalysis B: Environmental

journal homepage: www.elsevier.com/locate/apcatb

Review

The role of lanthanides in TiO_2-based photocatalysis: A review

Paweł Mazierski[a], Alicja Mikolajczyk[a,b], Beata Bajorowicz[a], Anna Malankowska[a], Adriana Zaleska-Medynska[a], Joanna Nadolna[a,*]

[a] Department of Environmental Technology, University of Gdansk, 80-308, Gdansk, Poland
[b] Laboratory of Environmental Chemometrics, University of Gdansk, 80-308, Gdansk, Poland

ARTICLE INFO

Keywords:
Photocatalysis
TiO_2
Lanthanides
Up-conversion process

ABSTRACT

This review provides an in-depth analysis of lanthanide-titania-modified semiconductor photocatalysts (Er-, Ho-, Nd- and Tm-TiO_2) for the photocatalytic degradation of organic pollutants under UV and visible light irradiation. In the first section, the unique properties of the lanthanides are summarized. In the second section, the influence of the preparation methods and surface properties of the selected rare earth metals (RE) on the photocatalytic activity of TiO_2 was surveyed. In the third section, the mechanism of the RE-TiO_2 visible light photoactivity was described. Finally, first-principles computer simulations of the RE-TiO_2 structure and energy along with the influence of the anti-Stokes up-conversion process on the photocatalytic activity of the RE-TiO_2 were discussed in detail.

1. Introduction

In recent years, environmental contamination has become a fundamental problem worldwide. In this regard, photocatalysis has been proposed as an environmentally friendly approach and a promising method to remove pollutants from water and air due to the possible oxidation of organic pollutants to CO_2 and H_2O. Titanium dioxide is the earliest discovered and most widely investigated photocatalyst as a result of its high photoactivity, relatively low cost, low toxicity and good chemical and thermal stability [1,2]. Unfortunately, TiO_2 is sensitive only to UV light by cause of its large band gap, and it has low quantum efficiency, resulting from the fast recombination rate of photogenerated electron–hole pairs. Various strategies of modifying TiO_2 have been applied to overcome the abovementioned drawbacks, such as metal and non-metal doping, surface modification by dyes, noble metal nanoparticles or narrow band gap semiconductor particles [1–14]. Among these strategies, the preparation of TiO_2 modified with rare earth (RE) metals appears to be a highly efficient method to tune the response of the semiconductor to the visible light region and to enhance its photocatalytic properties [15–18].The current reviews on rare earth metal-modified TiO_2 (RE-TiO_2) focus on the preparation methods and characterization of the photocatalysts [19], the photocatalytic degradation of organic molecules and the photosplitting of water in the presence of RE-TiO_2 [17], La, Ce, Eu, and Gd-TiO_2 [15], the use of Gd-TiO_2 for photoenergy applications [16], the use of RE-TiO_2 for the photocatalytic remediation of wastewater [18], visible-to-ultraviolet up-conversion processes [20] and thin lanthanides-TiO_2 films produced by spray-deposition [21]. However, it is still not clear how lanthanides affect visible light response of TiO_2-based photocatalysts. In view of this, this review covers important aspects related to the photocatalytic activity mechanism over selected (Er^{3+}, Ho^{3+}, Nd^{3+} and Tm^{3+}) RE-TiO_2 photocatalysts and the relationship between the mechanism and the anti-Stokes up-conversion process. Moreover, a computational description of the electronic structure and optical properties is provided to offer possible suggestions to researchers in this field for the design of new materials supported by computational methods. The preparation methods and surface properties of RE-TiO_2 are also discussed in detail.

2. Unique properties of lanthanides

Rare earth metals have shown great potential as TiO_2 dopants not only in the red shift of absorption but also in increasing the temperature of the anatase to rutile transformation and in the ability to form complexes with various Lewis bases, e.g., alcohols, aldehydes, acids, amines, and thiols [9,22,23]. Additionally, materials (such as TiO_2) modified by RE^{3+} ions usually present luminescent properties. Trivalent lanthanide ions with ladder-like energy levels embedded in an appropriate inorganic host lattice can emit UV or visible light through the sequential absorption of multiple near-infrared photons [20,24]. This process, which can result in the transformation of light from the near-infrared and visible spectral range to the ultraviolet wavelengths, could be used to excite wide band semiconductor, such as TiO_2 [25].

* Corresponding author.
E-mail address: joanna.nadolna@ug.edu.pl (J. Nadolna).

https://doi.org/10.1016/j.apcatb.2018.04.019
Received 9 December 2017; Received in revised form 10 April 2018; Accepted 12 April 2018
Available online 13 April 2018
0926-3373/

The lanthanides collectively consist of 15 elements starting with atomic number 57 (lanthanum) to 71 (lutetium). Scandium and yttrium are chemically similar; thus, finally 17 elements constitute the rare earth series. The luminescence of rare earth ions arises from the *f–f* electronic transitions within their partially filled 4*f* orbitals. These orbitals are sterically shielded from the surrounding microenvironment by the filled 5*s* and 5*p* orbitals, meaning that there are almost no perturbations of these transitions. Thus, these transitions appear as several narrow emission bands specific for the emitting lanthanide ion. This phenomenon gives the lanthanides unique chemical properties in photocatalytic applications [26,27]. Only four main lanthanide ions can theoretically activate the TiO_2 photocatalyst through the Vis-to-UV or NIR-to-UV up-conversion process, namely, Er^{3+}, Ho^{3+}, Nd^{3+} and Tm^{3+}. Simplified energy level diagrams of these RE ions and the excitation path for the up-conversion emission in the UV range are presented in Fig. 1. The up-conversion process can be achieved through the chains of the ground state absorption (GSA) and excited state absorption (ESA) [11]. During the anti-Stokes process, two or more photons are absorbed sequentially by a material to reach an excited state, and one higher-energy photon can be released [20]. For this reason, only the TiO_2 doped by Er, Ho, Nd and Tm was describe in the review and an attempt was made to correlate activity of these photocatalysts with their up-conversion properties.

3. Preparation methods and surface properties of RE-TiO_2

3.1. Erbium-TiO_2

3.1.1. Synthesis and morphology of Er-TiO_2

Generally, Er-TiO_2 can be obtained by hydro/solvothermal treatment, sol-gel methods and electrospinning, as shown in Table 1. Recent literature has revealed that the hydro/solvothermal and sol-gel methods are still some of the most commonly used synthesis methods for the preparation of Er-TiO_2 (see Table 1); these types of methods have become increasingly popular as straightforward, cost-effective preparation processes to produce Er-TiO_2 with high purity at a relatively low temperature.

In all applications, Er-TiO_2 photocatalysts have been employed in the form of various morphologies including zero-dimensional (nanoparticles), one-dimensional (nanotubes) or two-dimensional (nanobelts) structures, as shown in Figs. 2 and 3 and Table 1. These morphologies determine the physical and structural properties of RE-TiO_2 as well as its luminescence and photocatalytic properties. To prepare Er-TiO_2, titanium(IV) isopropoxide, titanium(IV) butoxide, TiO_2 colloidal solution can be used as TiO_2 precursors, while Er $(NO_3)_3{\cdot}xH_2O$, $ErCl_3$ and Er_2O_3 could serve as erbium precursors [28–35].

Among all the synthesis methods, magnetron sputtering [36], spin coating [37], implantation [38], and anodic [10,39] and thermal plasma oxidation [40] are infrequently used. Most of these methods (such as spin coating and magnetron sputtering) produce Er-TiO_2 photocatalysts as a thin layer. Moreover, the electrochemical oxidation of Ti foil in the presence of $Er(NO_3)_3$ in the ammonium fluoride/ethylene glycol organic electrolyte, allows formation of oriented nanotube arrays modified with erbium ions (one dimensional) [39].

In addition, most of the doping strategies have no influence on the morphology of the obtained Er-TiO_2; thus, a direct comparison of the photoactivity between the pristine and modified samples is reliable. However, in some cases, the morphology of the TiO_2 photocatalyst appears to be slightly influenced by the presence of Er ions. Obregón and Colón [41] found that the synthesis route they applied for the preparation of Er-TiO_2 photocatalysts produces a homogeneous distribution of round particles with sizes below 15 nm, but as the Er^{3+} content increases, the average size progressively decreases, reaching a value of 10 nm for 4 at.% Er^{3+}.

3.1.2. Crystal structure of Er-TiO_2

It is well known that one of the major factors that greatly influences the properties of the modified photocatalysts is the crystal structure, namely, the crystallite size and unit cell parameters. Yang et al. [42] prepared Er-doped TiO_2 nanofibrous films via an electrospinning method and observed that the crystallite size decreased from 17.9 to 8.1 nm as the erbium content introduced into TiO_2 increased from 0 (pristine) to 1.5 mol% (doped). They also found that the cell parameters of Er-TiO_2 were similar to pristine TiO_2. These results demonstrated that Er^{3+} species exist at the crystal boundary rather than in the inner crystalline structure of TiO_2 due to the substitution of a small Ti ion (68 pm) by a large Er ion (100 pm) causes an increase in the lattice parameters and a shift in the diffraction patterns [42]. A similar effect was found by Falcomer et al. [44] in which the crystallize size decreased from 30 to 16 nm after erbium doping, while the unit cell volume for the Er-TiO_2 sample was close to that of the pristine anatase TiO_2. The observed changes were attributed to the presence of lanthanide ions in the TiO_2 host, which led to strain and stress in the lattice [44]. Note that Li et al. [39] prepared Er-doped TiO_2 nanotubes and observed that the diffraction peaks of the doped photocatalyst moved to the left. Based on Bragg's law, they concluded that the left translation of the diffraction peaks indicated that the Er^{3+} was successfully introduced into the lattice of the TiO_2 nanotubes [39].

Another crucial point that should be mentioned, it is the effect of erbium doping on the hindrance of the phase transition of anatase to rutile. Several reports have demonstrated this phenomenon, when erbium ions were incorporated into TiO_2 lattice [41,42]. Yang et al. [42] observed that doping by erbium ions inhibited the appearance of the rutile phase when calcined at the same temperature 500 °C. It was proposed that this inhibition may occur due to the stabilization of the anatase phase by the surrounding rare earth elements through the formation of Ti–O-rare earth element bonds. The interaction between the different tetrahedral Ti atoms or between the tetrahedral Ti and the octahedral Ti prevents the phase transformation into rutile [42].

3.1.3. BET surface area and optical properties of Er-TiO_2

In reference to the BET surface area, Er–TiO_2 photocatalysts exhibit relatively high values; in all cases, the surface area was slightly higher than that of pristine TiO_2 (see Table 1). It was observed that the BET surface area progressively increased as the erbium content increased from 102 (for pristine TiO_2) to 116 m^2/g (for TiO_2 containing 4 at.% of Er) [41]. At the same time, it was observed that the pore size presents a narrow distribution, with an average pore size of 9–12 nm with increasing average values as the erbium content increased [34]. In contrast to the BET surface area, the literature data did not provide clear information about the band structure of erbium-modified TiO_2 photocatalysts. Some authors have observed a decrease in the band gap of Er–TiO_2, while other authors have found that the calculated band gap of Er–TiO_2 appeared to be similar to that of pristine TiO_2 (see Table 1). Therefore, the presence of erbium may or may not affect the band structure of the anatase structure. For example, Obregón et al. [34] and Mazierski et al. [10] found that erbium doping did not notably affect the absorption edge of TiO_2. Furthermore, they observed a small and progressive blue shift (after doping). A similar effect was also observed by Yang et al. [42] in which Er-TiO_2 photocatalysts were prepared using an electrospinning technique. These results are opposite to those found by Castaneda-Contreras et al. [31] for Er–TiO_2 systems prepared by the sol–gel method. They suggested that the incorporation of erbium into the structure induced a marked redshift and the subsequent narrowing of the band gap values. The improvement in the photoactivity was mainly attributed to the lower band gap values and, to a lesser extent, to energy transfer from Er^{3+} to TiO_2. Comparable results to that of Castaneda-Contreras et al. [31] were observed by Lee et al. [37]; namely, the energy gap values were 3.25, 2.85, 2.85, 2.85, 2.81, and 2.89 eV for 0, 0.1, 0.3, 0.5, 0.7 and 1.0 mol% of Er, respectively. In conclusion, the literature data are not consistent, and this aspect should

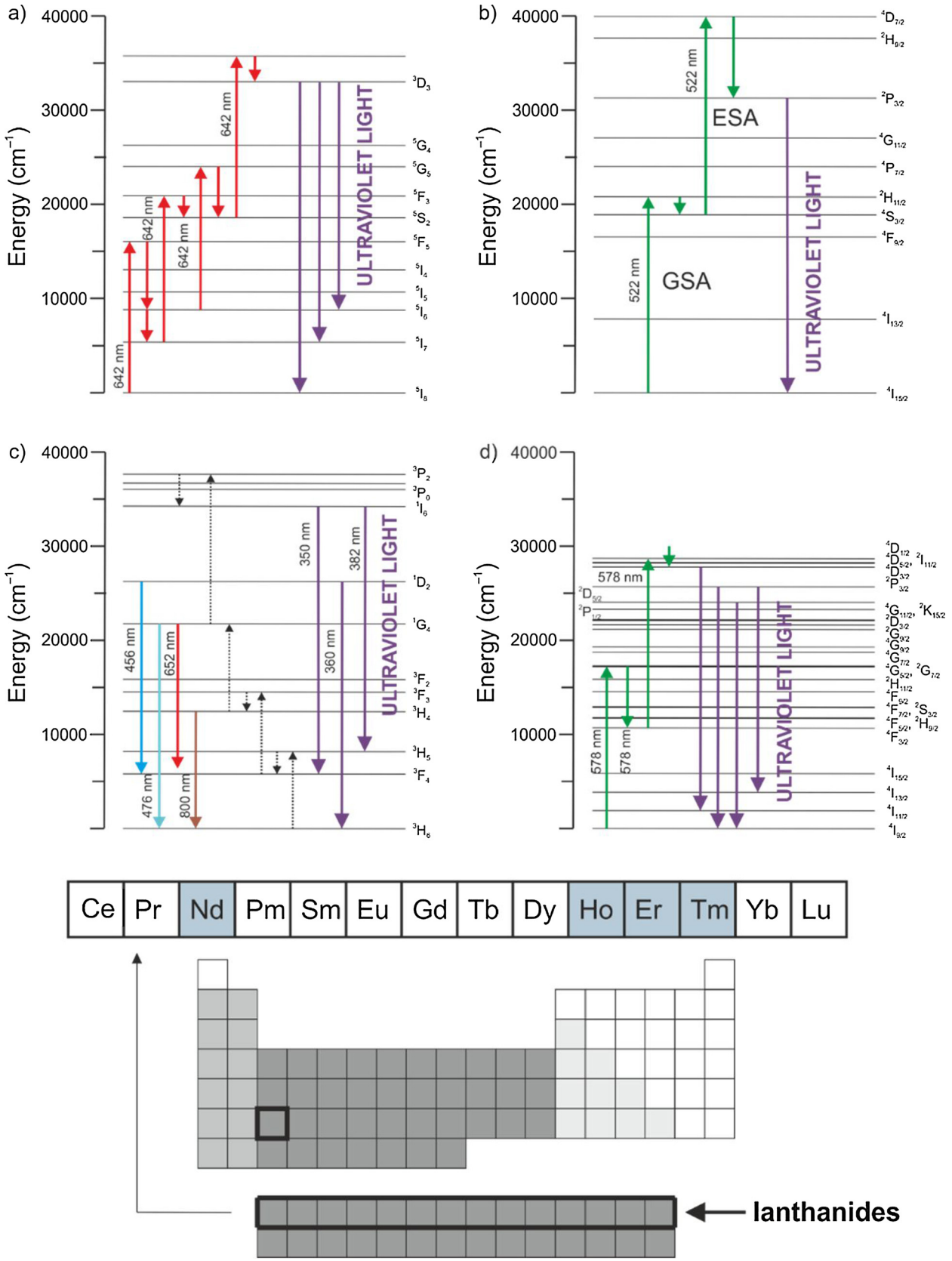

Fig. 1. Simplified energy level diagrams of an excitation path for the up-conversion emission of ultraviolet light: a) Ho^{3+} under 642 nm excitation, b) Er^{3+} under 522 nm excitation, c) Tm^{3+} under 980 nm excitation, and d) Nd^{3+} under 578 nm excitation; GSA - ground state absorption, ESA - excited state absorption.

Table 1
The structural and physical properties of Er-TiO_2 photocatalysts and description of photocatalytic system used to estimate photocatalytic activity.

No.	Preparation method/obtained structure	Localization of RE	Chemical characteristics of RE species	Unit cell parameters	BET Surface area (m^2/g)	Band-gap (eV)	Photocatalytic activity set -up	Up-conversion measurements	Ref.
1.	Sol-gel Thin film	Doping	Ion	No data	No data	No data	Not tested	λex = 800 nm λem = 410, 525, 548 and 660 nm	[45]
2.	Magnetron sputtering Thin film	Doping	Ion	No data	No data	No data	Not tested	λex = 980 nm λem = 490 and 670 nm	[36]
3.	Electrospinning Nanofibrous film	Doping	Ion	136.28 - pristine TiO_2 136.69 - Er-TiO_2	No data	Blue shift	**Model contaminant:** methylene blue **Irradiation source:** 500 W Xe lamp	Not tested	[42]
4.	Hydrothermal Nanoparticles	Doping (interstitial)	Oxidation state	136.30 - pristine TiO_2 136.35 - Er-TiO_2	102 - pristine TiO_2 110 - Er-TiO_2	3.16 - pristine TiO_2 3.18 - Er-TiO_2	**Model contaminant:** Phenol, toluene and methylene blue **Irradiation source:** 200 W Hg-Xe lamp (UV-Vis-IR, UV-Vis, Vis and Vis-IR)	λex = 980 nm λem = 390 and 415 nm	[34]
5.	Hydrothermal assisted sol-gel Nanopowder	Doping	Ion	No data	No data	No data	Not tested	λex = 980 nm Up-conversion was not detected	[35]
6.	Sol-gel Thin film	Doping	Ion	No data	No data	No data	Not tested	λex = 330 nm λem = 614 nm	[29]
7.	Solvothermal Nanoparticles	Doping (substitutional)	Ion	136.20 - pristine TiO_2 136.74 - Er-TiO_2	No data	No data	Not tested	λex = 488 nm λem = 550, 660 and 860 nm	[44]
8.	Hydrothermal Nanobelts	Doping	Ion	No data	No data	No data	Not tested	λex = 980 nm λem = 520-570 and 630-680 nm	[43]
9.	Sol-gel Nanoparticles	Doping (substitutional)	Ion	No data	No data	No data	Not tested	λex = 980 nm λem = 439, 488, 536, 565 and 664 nm	[30]
10.	Electrospinning	Doping	Ion	No data	No data	No data	**Model contaminant:** Phenol, methyl orange and rhodamine B **Irradiation source:** 500 W Xe lamp and LEDs (517-522 nm)	Not tested	[46]
11.	Electrospinning Nanofibers	Doping (substitutional)	Ion	No data	No data	Blue shift	Not tested	λex = 350 nm λem = 650 and 720 nm	[47]
12.	Sol-gel Nanoparticles	Doping	Ion	No data	No data	3.2 - pristine TiO_2 3.0 - Er-TiO_2	**Model contaminant:** Methylene blue **Irradiation source:** Deuterium-tungsten (Vis)	Not tested	[31]
13.	Thermal plasma oxidation Nanoparticles	Doping	New phase $Er_2Ti_2O_7$	No data	No data	No data	Not tested	Not tested	[40]
14.	Sol-gel Thin film	Doping (interstitial)	Ion	No data	No data	No data	Not tested	λex = 488 nm λem = 1534 and 613 nm	[32]
15.	Anodization Nanotubes	Doping (substitutional)	Ion	Increased	No data	No data	**Model contaminant:** Methylene blue **Irradiation source**: 160 W Hg lamp	Not tested	[39]
16.	Sol-gel Nanoparticles	Doping	Ion	No data	No data	Red shift	**Model contaminant:** Orange I **Irradiation source:** 8 W Hg lamp (UV) and 70 W sodium lamp (Vis)	Not tested	[33]
17.	Spin coating Thin film	Doping	Ion	No data	No data	3.25 - pristine TiO_2 2.81 - Er-TiO_2	Not tested	Not tested	[37]
	Hydrothermal Nanoparticles	Doping (substitutional)	Ion	No data	102 - pristine TiO_2 110 - Er-TiO_2	3.16 - pristine TiO_2 3.18 - Er-TiO_2	**Model contaminant:** Phenol and methylene blue **Irradiation source:** 200 W Hg-Xe lamp (UV-Vis-IR, UV-Vis, Vis and Vis-IR)	Not tested	[48]

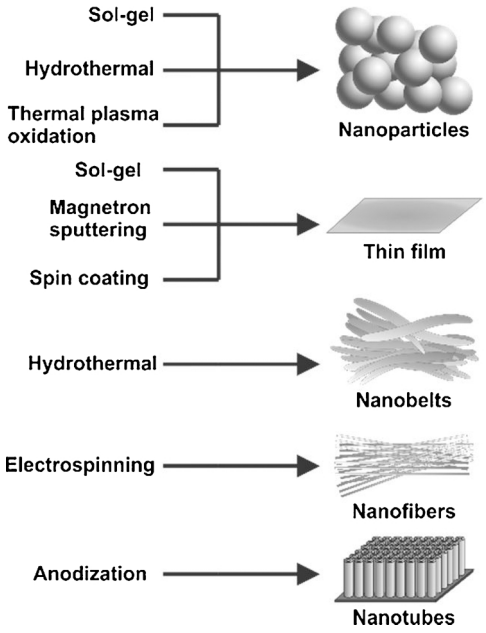

Fig. 2. Schematic illustration of the Er-TiO_2 morphologies obtained by sol-gel, hydrothermal, thermal plasma oxidation, spin coating electrospinning and anodization methods.

be clarified in the future. Additionally, for erbium-doped photocatalysts, different lines appear in the range of 400–700 nm compared to the TiO_2 absorption spectra, and those lines can be associated with the excitation of the erbium species. The absorption lines located at approximately 489, 520, and 653 along with a small tail at 800 nm correspond to the transitions from the Er^{3+} ground state $^4I_{15/2}$ to the higher energy levels of $^4F_{7/2}$, $^4H_{11/2}$, $^4F_{9/2}$ and $^4G_{9/2}$, respectively [31,33,34].

3.1.4. *Up-conversion properties of Er-TiO_2*

The up-conversion properties of the Er-TiO_2 photocatalysts have often been studied. In the case of NIR irradiation, the presence of erbium appears to promote the up-conversion process, pumping photons into the UV range in the TiO_2 structure (as shown in Fig. 2). It was reported that Er-TiO_2 shows a weak UV photoluminescence (PL) emission at approximately 390–410 nm after excitation at 980 nm [34]. This up-conversion process involves a sequential three-photon absorption ($^4I_{15/2} \rightarrow {}^4I^{11/2}$, $^4I_{11/2} \rightarrow {}^4F_{7/2}$ and $^4S_{3/2} \rightarrow {}^2G_{7/2}$). Then, by multiphoton relaxation, the $^2G_{7/2}$ excited state decays to the lower $^2G_{11/2}$ and $^2H_{9/2}$ states. The photoluminescence emission in the UV range is then produced by the $^2G_{11/2} \rightarrow {}^4I1_{5/2}$ transition, giving a feeble emission at approximately 390–400 nm [34]. Therefore, the improvement of the photocatalytic efficiency might be related to the increasing number of available photons with an appropriate energy. Obregón et al. [34] found that by exciting the Er-TiO_2 photocatalyst with 980 nm light, PL spectra in the UV region show two weak emission bands located at approximately 390/3.18 and 415/4.14 nm/eV. In contrast to these results, Mao et al. [36] observed only a 490 nm green emission and a 670 nm red emission after excitation of the Er-TiO_2 thin film by a laser of 980 nm. Bahtat et al. [28] studied the up-conversion properties of the Er-TiO_2 samples in the form of planar waveguides obtained by sol-gel method followed by dip-coating. In this case, four broad bands were observed at approximately 410, 525, 548, and 660 nm. However, Salhi and Deschanvres [35] obtained RE-TiO_2 nanopowders, which exhibited

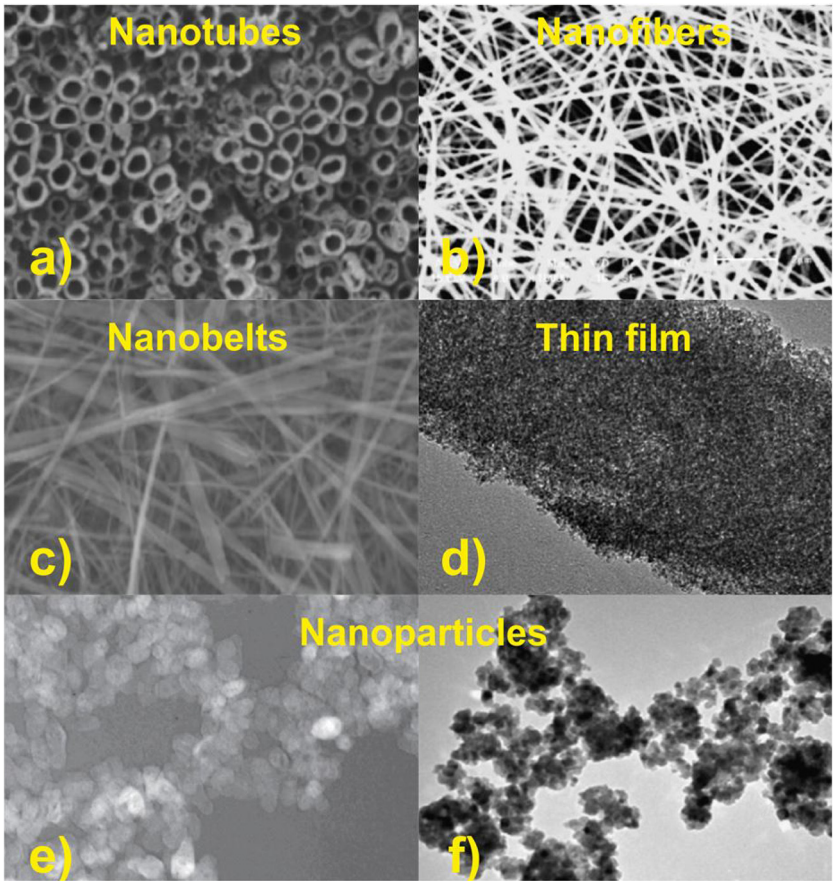

Fig. 3. (a–c) SEM and (d-f) TEM images of the Er-TiO_2 morphologies based on [30,32,34,39,42,43]. Reprinted with permission from ref [30,32,34,39,42,43]. Copyright 2009, 2010, 2012, 2014 Elsevier Inc.

strong, weak and very weak emission bands located at 550, 525 nm (green region) and 655 nm (red region), respectively. In summary, only Obregón et al. [34] observed a very frail emission band located at approximately 390 nm, which confirmed the up-conversion process proposed, whereby erbium converted the NIR photons to high-energy UV photons.

3.1.5. Photocatalytic properties of Er-TiO_2

The photocatalytic activity of the Er-TiO_2 photocatalysts was investigated under UV–vis, Vis and NIR irradiation using aqueous solutions of methylene blue (MB), phenol, methyl orange, rhodamine B, and orange I as model pollutants (see Table 1). These model reactions have been used to investigate both the effects of the erbium content incorporated into the TiO_2 structure as well as the calcination temperature on the photoactivity. Nonetheless, photocatalytic activity has been estimated using different set-ups and irradiation sources, such as 500 W xenon lamp, 200 W Hg-Xe lamp, deuterium-tungsten lamp, 160 W high-pressure mercury lamp, 8 W medium-pressure mercury lamp and light-emitting displays (LEDs) (Table 1). The effects of the erbium content incorporated into the TiO_2 structure and the calcination temperature on the photoactivity under solar simulated light using MB as the model pollutant was studied by Yang et al. [42]. It was shown that the photocatalytic activity of the erbium-doped TiO_2 was higher than that of pristine TiO_2 under simulated solar light [42]. The transition of the *4f* electrons of Er^{3+} enhanced the optical adsorption of photocatalysts and benefitted the separation of photogenerated electron-hole pairs [42]. TiO_2 doped with 0.5 mol.% of erbium possessed the highest photocatalytic achievement, and the photoactivity diminished by increasing the doping dosage. It was stated that resulted lower photoactivity was due to higher number of recombination centers because surplus amounts of RE metals cover the surface of TiO_2 [42]. In the case of the calcination temperature, the authors observed that the photoactivity of the photocatalysts prepared from 400 to 700 °C decreased [42]. Combining these results with the crystalline phase of TiO_2, indicates that the presence of the rutile phase (detectable under a higher calcination temperature) was responsible for the lower photocatalytic activity in the photodegradation of organic compounds [42]. Reszczyńska et al. [8] reported characteristics of Er-TiO_2 photocatalysts obtained via hydrothermal and sol-gel route. A high photocatalytic performance in the phenol photodegradation under visible light irradiation ($\lambda > 420$ nm) was observed for photocatalysts prepared by the hydrothermal method [8]. All RE–TiO_2 samples synthesized by the hydrothermal method had higher BET surface area and lower crystallite size than that developed by the sol–gel technique. Notwithstanding, photocatalysts prepared by the sol–gel method contained higher amounts of RE_2O_3 on their surfaces and fewer OH− groups and Ti^{3+} moieties than the powders produced via the hydrothermal method [8]. The effect of the erbium content incorporated into the TiO_2 structure on the photoactivity was also investigated by Zheng and Wang [46]. They found that the optimal dopant loading equaled to 1 mol.%, which correspond to the maximum photocatalytic degradation rate [46]. Furthermore, the photodegradation of rhodamine B and phenol under LED irradiation (λ = 517–522 nm) demonstrated that Er-TiO_2 photocatalysts can show photocatalytic activity under visible light beyond the absorption edge of TiO_2. Obregón et al. [34] studied the photocatalytic performance of the Er-TiO_2 photocatalysts in the model reactions of phenol and MB in the aqueous phase and toluene in the gas phase degradation in the presence of irradiation with different spectral ranges of the lamp (UV, Vis and/or NIR). In this study, better photon efficiencies have been found for the reaction under NIR irradiation than under UV conditions. UV-induced photoactivity was assigned to electrons trapping by Er^{3+} ions working as scavengers, while photocatalytic activity under NIR was ascribed to the up-conversion properties of the Er-TiO_2 photocatalysts, resulting in pumping photons in the UV range into the TiO_2 structure. Castaneda-Contreras et al. [31] studied Er–TiO_2 photocatalysts prepared by the sol–gel method in the reaction of MB degradation under visible light. They suggested that incorporation of erbium into the structure induces a marked red shift and a subsequent narrowing of the band gap values [31]. The improvement of the photoactivity was mainly attributed to the narrower band gap and, to a lesser extent, to energy transfer from Er^{3+} to TiO_2 [31]. To evaluate the photocatalytic activity of as-prepared samples, the kinetics of orange I photocatalytic depletion using Er–TiO_2 photocatalysts has been studied [33]. The obtained results demonstrated that the degradation and mineralization of orange I under both UV and visible radiation were more efficient in the presence of Er–TiO_2 photocatalysts than in the presence of pristine TiO_2. The authors concluded that the higher activity upon visible light might be attributed to the transition of the *4f* electrons of Er^{3+} and the red shifts of the optical absorption edge of TiO_2 by erbium ion doping [33]. Bhethanabotla et al. [49] studied Yb/Er-TiO_2 photocatalysts in the reaction of phenol and Rose Bengal photodegradation under simulated solar irradiation and irradiation at different narrow wavelengths (405, 530, 660 and 940 nm). They observed that phenol and Rose Bengal was degraded only by irradiation using wavelength equaled to 405 nm. The enhanced photoactivity was described to photon energy of the excitation source relative to the band-gap and differences in defect chemistry instead of to up-conversion effect. On the other hand, Pickering et al. in their investigation [50] displayed that neither up-conversion decreased recombination rate nor band gap modification, but increased contaminants adsorption at the surface of photocatalysts was the most important reason for the improved performance of erbium based-TiO_2.

Finally, to enhance visible light response of Er-TiO_2 and thus photodegradation of pollutants, some additional modifications of these photocatalysts have been applied, such as carbon-sensitization and Fe-Er co-doping [51], Er–Yb co-doping [52] and composite systems, including YAG:Yb^{+3},Er^{+3}/ TiO_2 [50], YSO:Pr^{3+}/TiO_2 and YAG;Er^{3+}/TiO_2 [53].

3.2. Holmium-TiO_2

The structural, physical and photocatalytic properties of Ho-TiO_2 photocatalysts are summarized in Table 2. To develop Ho-TiO_2 photocatalysts in the form of zero-dimensional (nanoparticle) and one-dimensional (nanowire) morphologies, two most common methods, namely, the sol-gel and hydrothermal methods, respectively (see the third column in Table 2), have been employed. Regarding the morphology of Ho-TiO_2, Cai et al. [54] found that the Ho-TiO_2 nanoparticles had relatively uniform spherical grains, a narrow size distribution, and good dispersity compared with pristine TiO_2 nanoparticles, indicating that holmium doping could improve the particle morphology and hinder the grain growth of TiO_2 upon heat treatment. Also in the case of photocatalysts prepared by Shi et al. [55] the particle diameter of holmium-doped TiO_2 was smaller than pristine TiO_2, and moreover Ho-doped TiO_2 presented an anomalistic sphericity. Zhou et al. [56] described Ho-TiO_2 photocatalysts in the form of nanowires made using hydrothermal route. They found that nanowires with a uniform dispersion and with an outer diameter and length of 15 nm and 500 nm, respectively, have been formed at 150 °C [56]. Regarding the crystal structure, similarly to Er-TiO_2, holmium doping effectively inhibits the further transformation from anatase to rutile. The inhibition of the phase transition might be ascribed to the stabilization of the anatase phase by the surrounding rare earth ions through the Ti−O−Ho interaction [54,55]. It was also observed that the crystallite size of the Ho-TiO_2 decreased with an increase in the holmium doping amount [54]. Furthermore, studies have shown that the crystallite size increased with the increase of calcination temperature, which implied that holmium doping inhibited the growth of the crystallite size [55]. Shi et al. [55] stated that the BET surface area also increased after holmium doping due to the decrease of the crystallite size. Another important aspect of Ho-TiO_2 photocatalysts is the disturbing of band gap structure. Shi et al. [57] observed a tiny blue shift

Table 2
The structural and physical properties of the Ho-TiO_2 photocatalysts and description of photocatalytic system used to estimate photocatalytic activity.

No.	Preparation method/obtained structure	Localization of RE	Chemical characteristics of RE species	Unit cell parameters	BET Surface area (m^2/g)	Band-gap (eV)	Photocatalytic activity set -up	Up-conversion measurements	Ref.
1.	Sol-gel Nanoparticles	Doping	Ion	0.1360 - pristine TiO_2 0.1365 - Ho-TiO_2	No data	No data	**Model contaminant:** methyl orange **Irradiation source:** Mercury lamp	Not tested	[54]
2.	Sol-gel Nanoparticles	Doping	Ion	0.1225 - pristine TiO_2 0.1235 - Ho-TiO_2	No data	No data	**Model contaminant:** methyl orange **Irradiation source:** 500 W high-pressure mercury lamp	Not tested	[57]
3.	Sol-gel Nanoparticles	Doping	Ion	0.1234 - pristine TiO_2 0.1245- Ho-TiO_2	38.42 - pristine TiO_2 76.76 for - Ho-TiO_2	No data	**Model contaminant:** methyl orange **Irradiation source and range:** 500 W high-pressure mercury lamp	Not tested	[55]
4.	Hydrothermal Nanowires	Doping	Ion	No data	No data	No data	**Model contaminant:** methylene blue **Irradiation source and range:** 175 W high pressure mercury lamp	Not tested	[56]
5.	Anodization Nanotubes	Surface doping	Oxide	136.64 - pristine TiO_2 136.73 - Ho-TiO_2	No data	3.35 - pristine TiO_2 3.30 - Er-TiO_2	**Model contaminant:**Phenol and toluene **Irradiation source and range:** 1000 W Xe lamp and LEDs (465 nm)	λex = 375, 530, 650 and 980 nm λem = not observed	[10]

of the absorption profile in the Ho-TiO_2 compared to pristine TiO_2. This blue shift was also observed by Cai et al. [54] and was ascribed to the quantum size effect because Ho-doping greatly suppressed the crystal size of TiO_2. In contrast, a slight red shift of the absorption profile in the range of 300–450 nm was observed in the Ho-TiO_2 nanowires by Zhou et al. [56]. The authors ascribed these results to the charge transfer transition between the f electrons of Ho^{3+} ions and the TiO_2 conduction or valence band. The absorption edge shifted to a longer wavelength, which was dependent on the amount of Ho^{3+} incorporated into TiO_2 lattice [56]. According to the available literature, the photocatalytic properties of the Ho-TiO_2 photocatalysts were investigated mainly only upon UV–vis irradiation using a high-pressure mercury lamp as an excitation source and using dyes (methyl orange and MB) as the model pollutants (see Table 2). In all the studies, the photocatalytic activity of the Ho-TiO_2 photocatalysts was obviously higher than that of pristine TiO_2 [10,54]. The better performance of Ho-TiO_2 has been explained by the fact that the Ho-doped photocatalysts have a smaller crystallite size and can enhance the separation efficiency and inhibit the recombination efficiency of the photogenerated electron-hole pairs [56,57]. Moreover, the expansion in the crystal matrix creates oxygen vacancies, which generate shallow energy states at the bottom of the conduction band and serve as electron-trapping sites in TiO_2 [54]. Meanwhile, shallow energy states introduced by Ho ions in the top valence band served as hole-trapping sites. The separation of the charge carriers was attributed to this trapping mechanism [56]. The optimal dopant amount equaled to 0.3 mol.% for the maximum photocatalytic degradation rate when Ho-TiO_2 was calcined at 500 °C, and the optimal calcination temperature was 600 °C when the holmium amount was 0.5 mol.% [54–57].

3.3. Thulium–TiO_2

There are only a few studies regarding thulium-doped or co-doped materials in different applications [58–61], although Tm-TiO_2 photocatalysts have received very little research attention (see Table 3). Tm-doped TiO_2 photocatalysts were synthesized using a low-temperature hydrolysis reaction [62,63] as well as a ball-milling method [64]. The effects of the annealing temperature as well as thulium doping amount on the structural and electronic properties of the obtained Tm-TiO_2 materials were investigated. Navas et al. [62] noted that anatase was the predominant phase in the Tm-TiO_2 samples annealed at 500 and 700 °C, while rutile was the main phase in the samples annealed at 900 °C. It is worth noting that the authors observed only the phase corresponding to TiO_2 for the samples annealed at 500 and 700 °C, while in the case of the sample annealed at 900 °C, the pyrochlore phase of $Tm_2Ti_2O_7$ was also obtained [62]. Santos et al. [63] showed that mixed oxides of Tm and Ti were formed in the case of the Tm-TiO_2 photocatalyst annealed at 900 °C. Therefore, the Tm^{3+} ion may be incorporated into the anatase structure but not into the rutile one, probably because the ionic radius of Tm^{3+} is considerably larger than that of Ti^{4+} and the anatase structure is less dense than the rutile one [62]. A similar observation was reported by Shlyakhtina et al. [65] who showed that, for $RE_2Ti_2O_7$ (where RE = Lu, Yb, Tm) samples, the pyrochlore structure was formed at temperature higher than 800 °C [8]. Thus, all the above studies indicated that the structure of the Tm-doped TiO_2 nanoparticles can be thermally controlled. Modification of titania with thulium led to an increase in the BET specific surface area of the obtained photocatalysts, but it was not the primary factor for improving the photocatalytic activity of Tm-doped TiO_2 samples [63,64]. Furthermore, XPS analysis confirmed the presence of Tm^{3+} in the Tm-TiO_2 samples, which led to the generation of structural distortions and oxygen vacancies to maintain the local neutrality in the lattice [62–64]. The presence of Tm^{3+} in the samples also influenced the changes in the UV–vis absorption spectra, probably because of the presence of new states in the band gap, which produces a new photonic absorption process and shows photoluminescence properties [62]. Santos et al.

Table 3
The structural and physical properties of the Tm-TiO_2 photocatalysts and description of photocatalytic system used to estimate photocatalytic activity.

No.	Preparation method/ obtained structure	Localization of RE	chemical characteristics of RE species	Unit cell parameters	BET Surface area (m^2/g)	Crystallite size (nm)	Band-gap (eV)	Photocatalytic activity	Up-conversion measurements	Ref.
1.	Low temperature hydrolysis reaction/ nanoparticles	Doping (substitutional)	Ion, oxidation state	V = 135.9 Å –pristine TiO_2 V = 128.9 Å-Tm-TiO_2	117.2-pristine TiO_2 274.6-Tm-TiO_2	13.1 - pristine TiO_2 5-Tm-TiO_2	3.01- pristine TiO_2 3.11- Tm-TiO_2	**Model contaminant:**methylene blue **Irradiation source and range:** 5 actinic lamps (λ = 360 nm)	Not tested	[62]
2.	Ball mill/ nanoparticles	Doping (substitutional)	Oxidation state	V = 62.1-pristine TiO_2 V = 135.9 Å-Tm-TiO_2	24.6-pristine TiO_2 51.8-Tm-TiO_2	57.2-pristine TiO_2 28.8-Tm-TiO_2	2.98- pristine TiO_2 2.93- Tm-TiO_2	**Model contaminant:**methylene Blue **Irradiation source and range:** actinic lamp (λ = 360 nm)	Not tested	[63]
3.	Water-controlled hydrolysis reaction/ nanoparticles	Doping (substitutional)	Ion, oxidation state	V = 62.4-pristine TiO_2 V = 62.5 Å-Tm-TiO_2	20.2-pristine TiO_2 23.0-Tm-TiO_2	69.9-pristine TiO_2 59.6-Tm-TiO_2	2.96-pristine TiO_2 2.96-Tm-TiO_2	**Model contaminant:**methylene blue **Irradiation source and range:** actinic lamps emitting (λ = 360 nm)	Not tested	[64]

[63] showed that Tm-doped samples presented several absorption bands centered at approximately 466, 685 and 785 nm, which corresponded to the transitions of Tm^{3+}. A similar observation was reported by Navas et al. [62], who showed that the intensity of these three absorption peaks increased with higher amounts of neodymium in Nd-doped TiO_2 samples. The photocatalytic activity of Tm-doped TiO_2 and pristine TiO_2 nanoparticles was estimated by examining the reaction of MB degradation under UV light irradiation using an actinic lamp emitting at approximately 360 nm [62–64]. Navas et al. [62] investigated the photocatalytic efficiency of pristine rutile TiO_2 as well as 2 and 4.3 at.% Tm-doped TiO_2 samples, which are composed of the rutile and anatase TiO_2 as well as pyrochlore $Tm_2Ti_2O_7$ phases. It was observed that the rate of the photocatalytic reaction using the thulium-doped TiO_2 samples was approximately 50% faster than the reaction using non-modified TiO_2. The higher photocatalytic efficiency of the doped samples was ascribed to the formation of heterojunction at the interface of the phases in the thulium-doped samples, which promotes the separation of the electron-hole pair as well as the good charge carrier mobility due to the presence of the pyrochlore phase. These experimental results were also confirmed by theoretical calculations, which revealed that the Ti—O—Ti angle in the pyrochlore phase was approximately 136° (Fig. 4a), and this property influenced the high photocatalytic activity of the pyrochlore phase because charge carriers can move easily in the lattice. Importantly, the charge density and ELF studies (Fig. 4b and c) displayed that the presence of the Ti—O—Ti bonds enabled good charge mobility in the pyrochlore phase [62]. Santos et al. [63] investigated the influence of the annealing temperature of Tm-doped TiO_2 samples on the photocatalytic activity. It was interesting to note that samples annealed both at 500 and 720 °C exhibited lower photoactivity than pristine TiO_2. However, all Tm^{3+}-doped samples annealed at 900 °C exhibited a significant improvement in the photoactivity (up to 94% degradation), 40% higher than the undoped TiO_2 [63], which was caused by the formation of a mixture of anatase, rutile and new pyrochlore $Tm_2Ti_2O_7$ phases [63]. In another study, the photocatalytic activity of the Tm-doped samples annealed at 900 was analyzed, and the reaction rate increased by a factor of 2.35 in the sample with 2.0 at.% Tm [64]. This result could be ascribed to the presence of pyrochlore, which is coincided with previous studies [62,63].

3.4. Neodymium–TiO_2

Different methods for the preparation of Nd^{3+}-doped photocatalysts have been proposed: sol gel [66–76], a microwave-assisted mild temperature route [77], low-temperature synthesis [78] as well as chemical co-precipitation peptization [79] and hydrothermal methods [80], as shown in Table 4. Up to this moment, the effect of the Nd content on the physical structure and photocatalytic activities of doped samples was systematically investigated. Wojcieszak et al. [71] observed that an increase in the neodymium amount in the Nd-TiO_2 samples resulted in an increase in the crystallite size of the photocatalysts. In contrast, Khalid et al. [81], as well as El-Bahy and co-workers [68], suggested that Nd doping might restrain the growth of the TiO_2 crystallites. In another study, Wang et al. [78] showed that titania crystallites decreased in size as the amount of doped neodymium ions increased, which was explained by the adsorption of the neodymium species on the surface of titania, resulting in the inhibition of TiO_2 crystallite growth. The differences in the ionic radii prevent the neodymium ions from effectively being incorporated into the crystal structure of TiO_2; thus, neodymium is probably localized at the surface of the TiO_2 nanocrystals [71,80]. It is also worth noting that the negligible change in the cell parameters and cell volume of the doped samples compared to pristine TiO_2 also implied that neodymium ions were dispersed on the surface of TiO_2 [66,74]. Moreover, Gomez et al. [77] showed that the incorporation of Nd modified the BET surface area of Nd-TiO_2 samples, depending on the number of Nd ions. Low loadings of Nd significantly

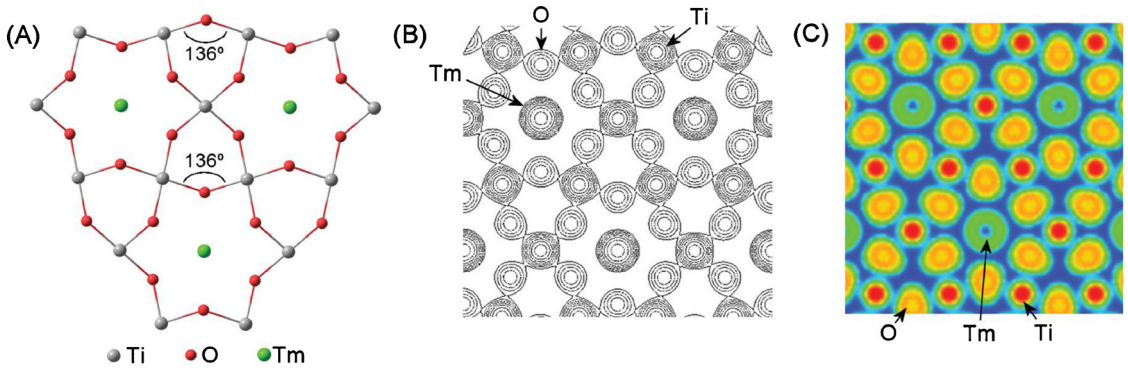

Fig. 4. (a) The local geometry, (b,c) analysis of the charge density and ELF for the pyrochlore phase ($Tm_2Ti_2O_7$) [62]. Reprinted with permission from ref [62]. Copyright 2014 The Royal Society of Chemistry.

increased the TiO_2 surface area, which was in good agreement with the results obtained by Hewer et al. [67] and Bokare et al. [66]. In contrast, a larger amount of Nd reduced the TiO_2 BET surface area, probably due to the blockage of some of the pores by the Nd clusters [77]. Kralchevska et al. [72] showed that modification of TiO_2 with neodymium significantly influenced the material texture, leading to increases in the BET surface area and micropore volume. It was also reported that modification of titania with neodymium greatly affected the light absorption property of the photocatalysts. Xu et al. [75] showed that the introduction of Nd extended the absorption spectrum of TiO_2 into the visible region and decreased the titania band gap, which was assigned to the charge transfer between the Nd ion *4f* level and the titania conduction or valence band. A similar observation was obtained by Wang et al. [78], who reported enhanced absorption properties of Nd-TiO_2 samples compared to pristine TiO_2 and observed five typical absorption peaks located at 527, 586, 762, 809 and 862 nm, which could be related to the *4f* electron transitions or the f-f transition of the Nd ions.

Furthermore, it was shown that doping by neodymium can affect the morphology of the TiO_2 particles. Bokare et al. [66] observed that undoped TiO_2 presented irregularly sized and shaped particles, while in the case of Nd-doped samples, particles with a more uniform size and shape were observed. Wojcieszak et al. [71] showed that undoped titania nanoparticles formed agglomerates, while the incorporation of the neodymium dopant in the amounts of 1 at.% and 3 at.% caused the TiO_2 agglomerates to become smaller. The addition of neodymium ions has been shown to increase the photocatalytic activity of titania for the removal of methyl orange [66,67,71,75], phenol [80,77,79], Remazol black B [79], direct blue 53 [68], reactive brilliant red X-3B [78], 2-mercaptobenzothiazole [70], malachite green [72], and rhodamine B [76], as well as the photoreduction of chromium (VI) [74] (see Table 4). It was reported that an appropriate amount of Nd-dopant played a crucial role in determining the photocatalytic activity of Nd-TiO_2 samples toward methyl orange decomposition, and an optimum amount of dopant in this system equaled to 3 at.% neodymium [71]. Bokare et al. [66] revealed that the highest activity was observed for TiO_2 containing 1 at.% of Nd, which was 30% higher than for the undoped TiO_2. A similar result was obtained by Khalid and co-workers [81], who showed that the best photoactivity was recognized for a 1 at.% Nd-TiO_2 sample. It is also interesting to note that Gomez et al. [77] reported that the main factors affecting the phenol degradation were the amount of neodymium and the band gap structure, while the surface area was the crucial parameter in the case of rhodamine B degradation. Wang et al. [78] proposed a photocatalytic mechanism of Nd-doped TiO_2 in which the excited electron can transfer from the valence band of TiO_2 to the newly formed neodymium energy levels below the conduction band of titania and can, therefore, be activated by visible light. Additionally, modification of TiO_2 with neodymium led to defects in the lattice, which acted as electron traps, resulting in an enhanced separation of charge carriers [78]. This result was in good agreement with the results obtained by Nassoko et al. [76], who reported that Nd entered into the TiO_2 lattice, and under visible light irradiation, the electrons were excited from the valence band to the Nd^{3+}/Nd^{2+} doping energy level. Additionally, it was found that hydroxyl radicals, as one of the reactive species, were produced by photogenerated electrons both from Nd-doped titania and rhodamine B and were mainly responsible for the photodegradation of the dye molecules [76]. In another study, Parnicka et al. [80,82] performed measurements of photocatalytic degradation in the presence of scavengers, and the results implied that e^- and $O_2^{\bullet-}$ were responsible for the photocatalytic degradation of phenol in the presence of Nd-TiO_2 samples under visible light irradiation. Furthermore, the action spectra analysis showed that Nd-TiO_2 samples could be activated by visible light with a wavelength range from 400 to 480 nm, suggesting that the up-conversion process of visible to ultraviolet light was not responsible for the visible light-driven photoactivity of Nd-TiO_2 photocatalysts [80].

4. The origin of RE-TiO_2 visible light photoactivity

4.1. Theoretical study of lanthanides-TiO_2 photocatalysts

4.1.1. Basic principles of the theoretical study of lanthanides-TiO_2 photocatalysts

Quantum chemical calculations are inexpensive and fast methods that can provide a description of the electronic and optical properties of surface-modified TiO_2 systems at the design stage (before synthesis) of new photocatalysts. The results from these theoretical calculations might provide important information for understanding and predicting the influence of RE metals on the electronic and atomic structure of RE-doped TiO_2 properties [83]. The most promising approaches that can be applied for this purpose are related to density functional theory (DFT methods) [83]. DFT theory can overcome the challenge related to investigating electronic structures in solid-state physics; more importantly, it is an effective approach for predicting the trend of the energy gap variation in doped semiconductors [83]. Despite the extensive experimental studies of RE-TiO_2 (as shown in Tables 1–4), there is a serious problem in the description of the effects of impurities on the TiO_2 photocatalyst performance. Thus, theoretical groups have reported numerous calculations to predict the properties of the complex RE-TiO_2 systems to provide more valuable insight into the experimental preparation that could improve the photoresponse activity from the UV to the Vis light region (as summarized in Table 5). On the basis of the first-principles calculations, the theoretical results show that the localized *4f* states of lanthanide ions (RE^{3+}) commonly result in band gap narrowing and photoresponse improvements under the visible light region [10,84]. Thus, in this part, we summarized the theoretical calculation of the electronic structure, charge density, and optical properties of RE^{3+}-doped TiO_2 systems. The mechanism of the enhanced

Table 4
The structural and physical properties of Nd-TiO_2 photocatalysts and description of photocatalytic system used to estimate photocatalytic activity.

No.	Preparation method/ obtained structure	Localization of RE	Chemical characteristics of RE species	Crystallite size (nm)	BET Surface area (m^2/g)	Unit cell parameters	Band-gap (eV)	Photocatalytic activity	Up-conversion measurements	Ref.
1.	Sol–gel/	Doping (interstitial)	Ion, oxide	20.759- pristine TiO_2	108.7 - pristine TiO_2	a = 3.786 nm, b = c = 9.507 nm, V = 136.315 Å3 - pristine TiO_2	No data	**Model contaminant:**methyl orange	λex = 345 nm	[66]
	nanoparticles			7.598- Nd-TiO_2	123.4- Nd-TiO_2	a = 3.778 nm, b = c = 9.532 nm, V = 136.629 Å3 - Nd-TiO_2		**Irradiation source and range:** direct sunlight (4% UV and 43% visible light)	λem:- 410,- 450,- 475 and- 520 nm	
2.	Mild microwave-assisted/ nanoparticles	Doping (interstitial)	Ion	6.92 - pristine TiO_2	239 - pristine TiO_2	a = 3.80 Å, c = 9.64 Å - pristine TiO_2	2.95 - pristine TiO_2	**Model contaminant:**phenol	Not tested	[77]
				5.79 - Nd-TiO_2	258- Nd-TiO_2	a = 3.80 Å, c = 9.61 Å - Nd-TiO_2	2.89- Nd-TiO_2	**Irradiation source and range:** medium pressure mercury lamp (λmax = 365 nm).		
3.	Sol–gel and precipitation/ nanoparticles	Doping	Ion, oxide	19.3 - pristine TiO_2	81 - pristine TiO_2	No data	No data	**Model contaminant:**remazol black B	Not tested	[67]
				12.3 - Nd-TiO_2	127.1- Nd-TiO_2			**Irradiation source and range:** high pressure mercury lamp (λ < 400 nm)		
4.	Sol –gel/ nanoparticles	Doping	Ion, oxidation state	29.5 - pristine TiO_2	223- pristine TiO_2	No data	3.27- pristine TiO_2	**Model contaminant:**direct blue 53	Not tested	[68]
				22.6- Nd-TiO_2	312- Nd-TiO_2		3.25- Nd-TiO_2	**Irradiation source and range:** xenon lamp (λ > 320 nm)		
5.	Sol–gel/monolith	Doping (substitutional) and intercalation	Ion	No data	72.6- pristine TiO_2	No data	3.10 - pristine TiO_2	**Model contaminant:**methyl orange	Not tested	[69]
					74.9- Nd-TiO_2		2.96 - Nd-TiO_2	**Irradiation source and range:** Xenon lamp **(λ > 365 nm)**		
6.	Sol-gel	Doping	Ion	32.9 - pristine TiO_2	50.2- pristine TiO_2	No data	No data	**Model contaminant:** 2-mercaptobenzothiazole	Not tested	[70]
				19.8- Nd-TiO_2	78.5- Nd-TiO_2			**Irradiation** source and range: medium-pressure mercury lamp (λ = 365 nm)		
7.	Sol-gel/ nanoparticles	Doping	Ion	4.2 - pristine TiO_2	No data	No data	No data	**Model contaminant:** methyl orange	Not tested	[71]
				4.6- Nd-TiO_2				**Irradiation source and range:** UV-Vis 20 W Phillips lamps		
8.	Sol–gel	Doping	Ion, oxidation state	29 - pristine TiO_2	7.3 - pristine TiO_2	a = 3.781 nm,	No data	**Model contaminant:** malachite green	λex = 330 nm	[72]
				7.6- Nd-TiO_2	57.7- Nd-TiO_2	c = 9.506 nm - pristine TiO_2 a = 3.791 nm, c = 9.505 nm - Nd-TiO_2		**Irradiation source and range:** UV lamp Sylvania, (345–400 nm, λmax: 365 nm)	λem = 521.0, 506.0, 495.1, 486.0, 442.1 and 421.2 nm	
9.	Sol-gel	Doping	Ion	32.9 - pristine TiO_2	43.29 - pristine TiO_2	No data	No data	**Model contaminant:** 2-mercaptobenzothiazole	λex = 325 nm	[73]
				17.8- Nd-TiO_2	90.91- Nd-TiO_2			**Irradiation source and range:** high-pressure sodium lamp (400-800 nm)	λem = 504, 539, 596 and 522 nm	

(*continued on next page*)

Table 4 (*continued*)

No.	Preparation method/ obtained structure	Localization of RE	Chemical characteristics of RE species	Crystallite size (nm)	BET Surface area (m^2/g)	Unit cell parameters	Band-gap (eV)	Photocatalytic activity	Up-conversion measurements	Ref.
10.	Chemical coprecipitation–peptization/ nanoparticles	Doping	Ion	No data	No data	No data	6	**Model contaminant:** phenol **Irradiation source and range:** halogen-tungsten lamp (400–800 nm, λmax = 550 nm)	Not tested	[79]
11.	Sol–gel/ nanoparticles	Doping	Ion	15.84 - pristine TiO_2 6.19- Nd-TiO_2	No data	a = 0.38 nm c = 0.95 nm - pristine TiO_2 a = 0.38 nm c = 0.95 nm- Nd-TiO_2	No data	**Photocatalytic reaction:** reduction of Cr(VI) **Irradiation source and range:** medium-pressure mercury lamp (325 nm)	Not tested	[74]
12.	Low temperature/ hollow spheres	Doping	Ion, oxide	No data - pristine TiO_2 8.9- Nd-TiO_2	No data	No data	No data	**Model contaminant:** reactive brilliant red X-3B **Irradiation source and range:** 250 W halogen lamp (λ > 400 nm) **Efficiency: 60.9% after 100 min**	Not tested	[78]
13.	Sol–gel and hydrothermal/ nanotubes	Doping (interstitial)	Ion, oxide	No data	No data	No data	No data	**Model contaminant:** methyl orange **Irradiation source and range:** high-pressure mercury lamp	Not tested	[75]
14.	Sol-gel/ nanoparticles	Doping (interstitial)	Ion, oxide	20.32 - pristine TiO_2 20.35- Nd-TiO_2	72.46 - pristine TiO_2 59.54- Nd-TiO_2	No data		**Model contaminant:** rhodamine B **Irradiation source and range:** Xenon Lamp (λ > 420 nm)	Not tested	[76]
15.	Hydrothermal	Doping	Ion, oxide	18.8 - pristine TiO_2 10.9- Nd-TiO_2	107 - pristine TiO_2 124- Nd-TiO_2	No data	No data	**Model contaminant:** phenol **Irradiation source and range:** Xenon Lamp (λ > 420 nm)	Not tested	[80]

Table 5
Computational details for the computed RE-TiO_2 structures available in the literature.

Type of structure	The k-point meshes used for geometrical optimizations	The plane-wave energy cutoff	The structural energy convergence/ the forces of relaxation	The valence atomic configurations	Methods	Software	Ref.
$Nd_2TiO_2O_7$	4 × 4 × 4 4 × 4 × 2 4 × 4 × 1	500 eV	self-consistent convergence of the total energy/ 0.01 eV/Å	Nd (5s25p66s25d1) Ti (3s23p63d24s2) O (2s22p4)	DFT-GGA + U (U = 7 eV) with PW	VASP	[88]
Nd^{3+}-TiO_2	Not provided	Not provided	Not provided	Not provided	DFT	Not provided	[84]
$Tm_xTi_{1-x}O_2$	x 7 x 3 2 × 3 × 3 x 3 × 3 2 × 4 × 1	400 eV	5.0×10^{-7} eV/atom/ 0.01 eV/Å	Tm (4f13 5s25p66s2) Ti (3s23p63d24s2) O (2s22p4)	DFT/ GGA with PAW	CASTEP	[89]
Ho-TiO_2	8 × 8 × 11 3 × 7 × 1 2 × 2 × 1	400 eV	< 1 meV/atom < 0.02 eV Å	Ho (4f115s25p66s2) Ti (3s23p63d24s2) O (2s22p4)	DFT/ GGA with PAW	VASP	[10]

band gap narrowing and the associated optical properties are also discussed in this section. It could be noted that up to this moment theoretical investigations on RE = Nd^{3+}, Tm^{3+}, Ho^{3+}, Er^{3+} doping are relatively rare.

4.1.2. Computational characterization of the investigated RE-TiO_2 structures

One of computationally investigates RE-TiO_2 system (i.e., $Nd_2Ti_2O_7$) was provided by Bruyer and Sayede in 2010 [85]. The authors indicated that the $Nd_2Ti_2O_7$ system could be applied in the water-splitting reaction and they reported the results from DFT methods on the structural optimization for Nd-TiO_2 in different atomic arrangements (Table 5) [85]. The room temperature arrangement of the investigated structure was monoclinic $P2_1$ with the lattice constants a = 13.02 Å, b = 5.48 Å, c = 7.62 Å and β = 98.28°. Bruyer and Sayede [85] provided results on the chemical bonding, structural phase stability and ferroelectronic properties, as well as the electronic structure of the Nd-TiO_2 system. The electronic structures of $Nd_2Ti_2O_7$ have been studied using the general gradient approximation method (GGA + U method). Based on GGA + U calculations and the density of states (DOS), the authors suggested a half-metallic nature for $Nd_2Ti_2O_7$ [85]. These results do not correspond to the experiment provided by Hwang et al. [86]. However, the GGA + U results moved the Nd 4*f* states away from the E_F, yielding an insulating ground state. The localized Nd 4*f* levels at the top of the valence band (VB) and at a lower position in the conduction band (CB) acted as charge-trapping sites, showing that the $Nd_2Ti_2O_7$ structure had a reduced photocatalytic activity [85]. Li et al. [87] observed band gap narrowing for the 0%, 1% and 1.5% Nd^{3+}-doped TiO_2 nanoparticles (NPs). To interpret the band gap (E_g) changes, the authors used the generalized gradient approximation (GGA) with the linearized augmented plane wave method (LAPW). The Nd-doped anatase was modeled by a structurally optimized $NdTi_7O_{16}$ supercell with Nd^{3+} in a substitutional site. Li et al. [87] indicated that the band gap narrowing was primarily attributed to the substitutional Nd^{3+} ions. Based on the obtained calculations, the authors indicated that Nd^{3+} ions introduced electron states into the band gap of TiO_2 (~ 2.26 eV), and these electron states influenced the new lowest unoccupied molecular orbitals (LUMOs). The calculated band gap of pristine TiO_2 equal to 1.97 eV, with the O *2p* orbital states contribution at the top of the VB and the Ti *3d* orbital contributions at the CB [87]. The calculated E_g of Ti_7NdO_{16} that corresponds to 4 at.% Nd equal to 1.97 eV, and from the DOS analysis, the authors concluded that some electronic states, which were located close to the CB, were introduced into the band gap of TiO_2 by Nd *4f* electrons to form the new LUMO [87]. Consequently, the absorption edge transition for the doped material can be from O *2p* to Nd *4f* instead of Ti *3d*, as in pristine TiO_2. Li et al. [87] observed that the maximum band gap reduction (E_g = 0.55 eV) was found for 1.5 at.% Nd-doped TiO_2 nanoparticles. Based on the obtained results, the authors indicated that E_g narrowing could be related to the substitutional Nd^{3+} ions, which introduced electron states into the band gap of TiO_2 to form the new LUMO [87].

Mazierski et al. [10] investigated the electronic structure and partial density of states (PDOS) of pristine TiO_2 and Ho-TiO_2. The electronic structure of the TiO_2 anatase system was changed by the defects in the photocatalyst surface and by the location of the Ho^{3+}. The Ho *f* states exist in the band gap of defective anatase TiO_2(101). The authors observed the system stabilization after the formation of defects at the surface of the Ho-anatase TiO_2(101) [10]. Wei and Jia [84] reported the electronic structure, charge density and optical properties of Tm^{3+}-modified TiO_2 based on DFT calculations (Table 5). The authors investigated three different configurations of the $Ti_{1-x}Tm_xO_2$ systems (see Fig. 5), in which the variation x was defined by the values of 0.0417, 0.0625, and 0.125. Tm atoms in $Ti_{1-x}Tm_xO_2$ systems were introduced into the regular Ti lattice position. The supercells were composed of multiples of the lattice vectors a, b, c, such as 3 × 2 × 1 (72 atoms), 2 × 2 × 1 (48 atoms), and 2 × 1 × 1 (24 atoms) supercells for the anatase phase $Ti_{1-x}Tm_xO_2$ system, which represented the doping concentrations of 1.39 at.% ($Ti_{23}O_{48}Tm_1$), 2.08 at.% ($Ti_{15}O_{32}Tm_1$) and 4.17 at.% ($Ti_7O_{16}Tm_1$), respectively [84]. The optical properties and electronic structures of the Tm-TiO_2 system were studied using the plane-wave DFT method with the Padrew-Burke-Ernzerhof-generalized gradient approximation functional (PBE/GGA) [84]. Wei and Jia [84] discussed the mechanism of the enhanced band gap (E_g) narrowing and the associated optical properties of the investigated Tm-TiO_2 system. Wei and Jia [84] observed the reduction of the band gap compared to pure anatase TiO_2 due to the incorporation of Tm into the anatase TiO_2 structure. The band gap was apparently reduced from 2.17 to 1.93 eV in the Tm-doped $Ti_{23}O_{48}Tm_1$ system. Consequently, Tm doping narrowed the band gap to a value of approximately ΔE_g = 0.24 eV [84]. For the Tm-doped anatase $Ti_{15}O_{32}Tm_1$ and $Ti_7O_{16}Tm_1$, the band gap energies, i.e., 1.92 eV (ΔE_g = 0.22) and 1.83 eV (ΔE_g = 0.29), corresponded to the doping levels of 2.08 at.% and 4.17 at.% of Tm atoms, respectively. Moreover, the presented results indicated that the Tm atoms substantially modified the DOS, inducing variations in both the VB and the CB [84]. The authors observed that the substitutional Tm dopant increased the delocalized Tm 4*f* states above the VB, which narrows the band gap, resulting in a red shift of the optical absorption edges [84]. A dependency between the Tm concentration and the band gap reduction was observed. The presented study was the starting point for the designed band-gap reduction using Tm-doped TiO_2 for extending the optical absorption into the visible solar light region for improved photocatalytic performance [84].

From the considered examples discussed in this paper, it appears that the theoretical description at the DFT level of the RE-TiO_2 semiconductor oxides presents a number of problems. Obtaining more accurate defect formation energies and a more reliable distribution of the excess electrons requires going beyond the GGA in DFT by using hybrid approaches; in general, this means increasing the computational

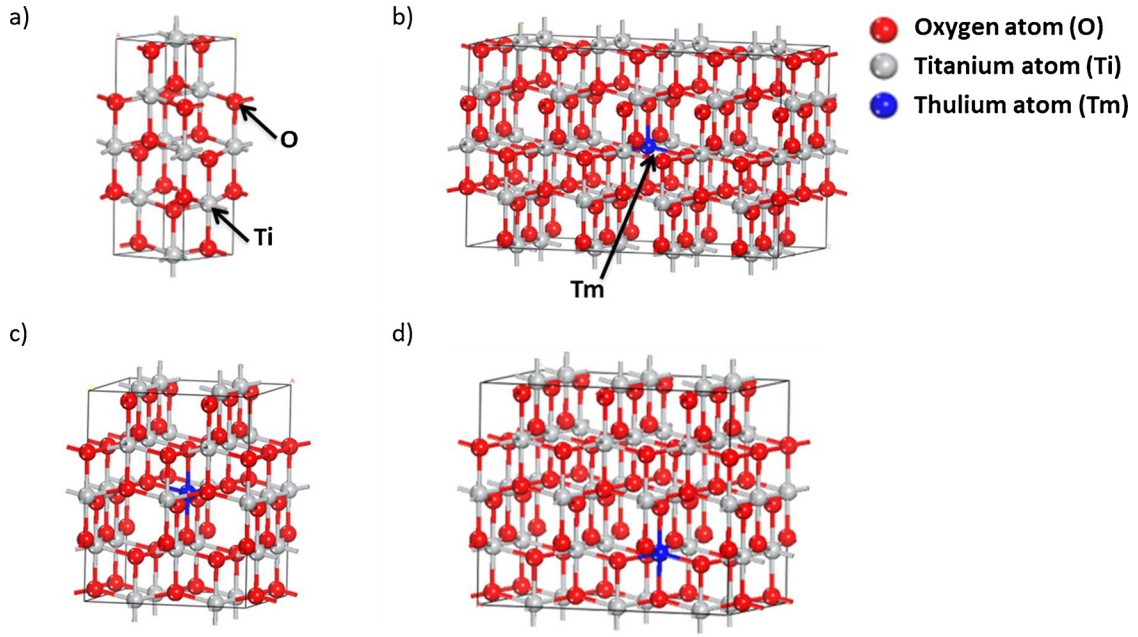

Fig. 5. The example investigated of the unit cell and doping model with substitutionally doped Tm atoms in the anatase TiO_2 supercells: (a) unit cell; (b) 3 × 1 × 1 supercell; (c) 2 × 2 × 1 supercell; and (d) 2 × 1 × 1 supercell. The red, gray and blue spheres represent oxygen, titanium, and thulium atoms, respectively, based on [84]. Reprinted with permission from ref [84]. Copyright 2015 Society of Photo-Optical Instrumentation Engineers (SPIE) (For interpretation of the references to colour in this figure legend, the reader is referred to the web version of this article).

demands. Thus, the choice of the model of the reduced system may become crucial. The question arises of whether widely used periodic models will be useful in this respect. Very recent studies on the electronic structure of defective TiO_2(110) surfaces using periodic models and hybrid functionals in [90] and [91] indicate that an increased interest can be expected in this type of calculation in the near future. However, cluster approaches will still be useful (and less costly computationally). Nonetheless, a universal hybrid functional that includes a fixed amount of the exact exchange might not necessarily be able to describe the electronic structure of all (different) RE-TiO_2 structures with the same accuracy.

4.2. Anti-Stokes up-conversion process in the RE-TiO_2 mechanism

The simplified mechanism of the TiO_2 excitation by the up-conversion luminescence agent is presented in Fig. 6.

To explain the possible mechanism of lanthanide-modified TiO_2 excitation under visible light, the photodegradation of model pollutants should be investigated as a function of irradiation wavelength (action spectra (AS) analysis) [8]. Based on AS analysis, it is possible to determine which aspect of light absorbed by the photocatalyst is involved in the photocatalytic reactions [80]. If the up-conversion process is involved in the improvement of the photocatalytic activity under visible light, then an enhancement of the photocatalytic activity in RE absorption bands region should be observed. In the recent literature, there are only a few reports of RE-TiO_2 AS measurements. Parnicka et al. [80] investigated the influence of the irradiation wavelength on the photocatalytic activity of the phenol degradation reaction in the presence of Nd-TiO_2 photocatalysts. The AS of the samples did not resemble the Nd-TiO_2 absorption spectra. The Nd-modified TiO_2 photocatalyst showed photocatalytic activity under visible light in a continuous irradiation range from 400 to 480 nm [80]. Photocatalytic activity under the Nd absorption band wavelengths (λ = 525, 585, 745, and 805 nm) was not observed (Fig. 7).

No correlation between the wavelengths responsible for the photocatalytic activity and the absorption spectra of RE was also observed by Reszczyńska et al. [9,11]; the photocatalysts Er-Yb-TiO_2, Nd-Eu-TiO_2

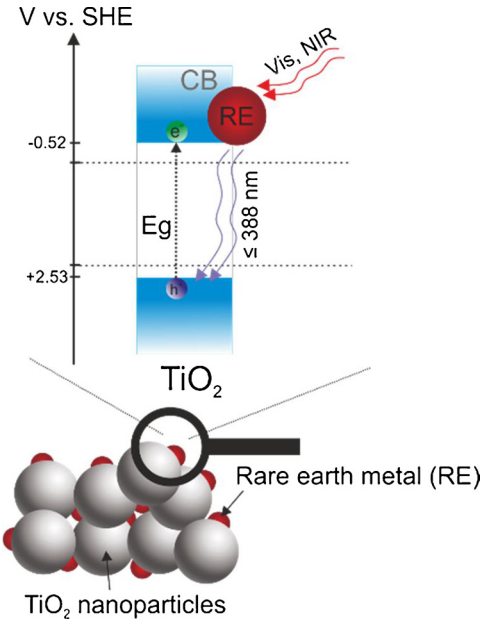

Fig. 6. Simplified mechanism of TiO_2 excitation by an up-conversion luminescence agent.

and Eu-Ho-TiO_2 showed photoactivity in the 420–475 nm, 420-450 nm and 420-450 nm regions, respectively. The enhancement of the photocatalytic activity under 488, 522, 524, 586 or 653 nm was not observed [9,11]. Different results have been obtained by Castaneda-Contreras et al. [31] who postulated that the up-conversion process in erbium ions was responsible for MB photodegradation under 532 nm laser beam light. According to recent literature, the reason that the impact of the up-conversion process on the photocatalytic activity was not always observed was because of the large distance between the ground and excited states of the RE ions (multiphoton excitation) and multiphonon

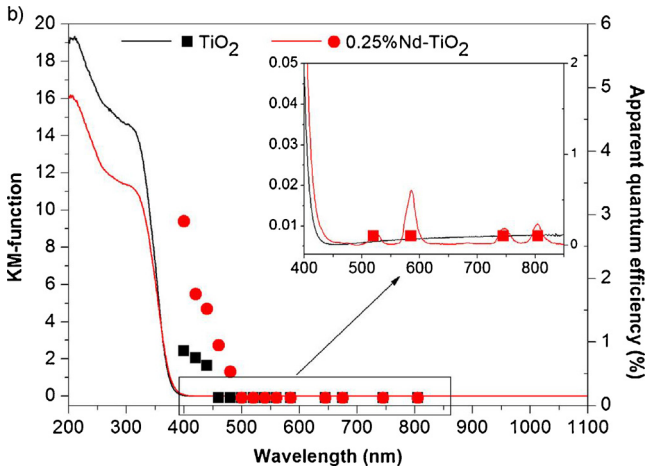

Fig. 7. Action spectrum of the photocatalytic degradation of phenol in the presence of neodymium-modified TiO_2 [80]. Reprinted with permission from ref [80]. Copyright 2017 Elsevier B.V.

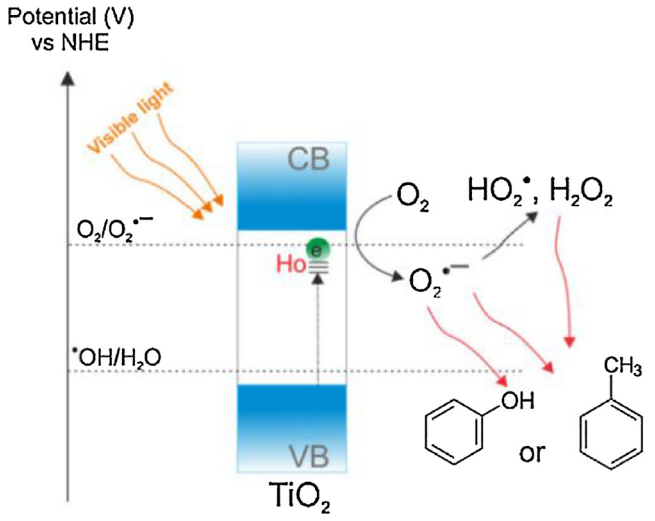

Fig. 8. Schematic illustration of the formation of sub-bandgap states below the conduction band of the TiO_2 semiconductor after the incorporation of Ho or Nd ions, based on [10,78]. Reprinted with permission from ref [10,78]. Copyright 2010, 2016 Elsevier B.V.

relaxation processes that were affected by the properties of the crystal structure of the photocatalysts [92,93]. Moreover, the aqueous environment of the solutions caused the interaction of RE with water (both in the inner and outer coordination spheres of the RE^{3+}) and led to a severe quenching of the RE luminescence via O—H vibrations [94]. The best way to minimize the water deactivation processes is to protect the RE^{3+} ion from solvent interactions, e.g., with a chelating process or by binding RE with peptides [94,95]. In the recent literature, there is no information regarding TiO_2 photocatalysts modified with RE ions with extra protection from aqueous interactions. Based on the literature, there is no reliable proof that the up-conversion process has a real impact on the RE-TiO_2 photocatalytic activity under visible light irradiation; therefore, this aspect should be clarified in the future. Mazierski et al. [10] and Wang et al. [78] stated that the incorporation of Ho or Nd ions into the TiO_2 structure leads to the formation of sub-bandgap states that lie below the CB of the semiconductor. The electrons can be excited from the VB to the lanthanide 4*f* level under visible light irradiation (as shown in Fig. 8). These trapped electrons can react with O_2 and form reactive oxygen species, such as $O_2^{\cdot -}$, HO_2 and H_2O_2, leading to organic pollutant degradation [10].

5. Conclusions and perspectives

Current review provides a comprehensive summary of the studies that investigated modification of TiO_2 with Er, Ho, Nd and Tm ions. Rare ions (RE) were used for the TiO_2 modification in order to obtain photocatalysts being active under visible light irradiation. In particular, dye degradation has been found to be a popular choice for the comparison of the photoactivity between pristine TiO_2 and RE-TiO_2. The aforementioned literature data suggests that RE-TiO_2 modification is effective in increasing the photocatalytic activity of TiO_2, especially at low loading levels. However, due to various photocatalytic activity set-ups chosen for the carried tests, the choice of a lanthanide causing the highest increase is challenging. According to the literature, there is no reliable proof that the up-conversion process has a real impact on the RE-TiO_2 photocatalytic activity under a visible light irradiation. Moreover, there is currently no information regarding TiO_2 photocatalysts modified with RE ions with extra protection from aqueous interactions in the recent literature. Therefore, those two aspects should be clarified in the future. What is more, time-consuming and often very expensive experimental testing, as well as substantial amount of the possible RE-TiO_2 structure combinations leads to limitations in proper characterization of RE-TiO_2 photocatalysts. It has been widely proved that theoretical calculations combined with chemoinformatics methods (i.e. Quantitative Structure-Property Relationship modeling, QSPR) may support the experimental testing of new potential photocatalysts [10,96–98]. However, an effective approach that combines theoretical and computational calculations with experimental design is still not well developed yet. Since organizing a synergistic interaction between experimentalists and theoreticians is a critical step, we proposed a roadmap (Fig. 9), showing which objectives need to be achieved in a short-, medium-, and long-term tasks. In the first step (i.e. short-term task) the following tasks are of highest importance: i) selection of well characterized materials for the experiments; ii) selection and measurements of activity-relevant endpoints (Fig. 9). When examining photocatalytic properties of RE-TiO_2 systems, it is important that electronic and atomic properties of TiO_2, RE particles and RE-TiO_2 systems are well characterized and understood, so that valid inferences can be gained, and how these structure properties influence the photocatalytic activity. Therefore, in the second step (i.e. medium-term task), a computational approach should be undertaken, where one of the most important components of theoretical methods are developed. The physico-chemical features, defined as descriptors can help in understanding the relationships between atomic structure and electronic/optical properties of investigated molecular models. In the long-term task, the database comprised of physico-chemical properties (i.e. descriptors) and photocatalytic activity measurements (i.e. endpoints) of investigated TiO_2 systems should be developed. Afterwards, on a basis of the gathered data, computational models (i.e. QSPR models for nanoparticles, nano-QSPR) for reliable endpoints should be developed, providing a knowledge how the photocatalyst structure affects its desired property (i.e. photocatalytic activity). Finally, the developed models should be used to preliminarily estimate photocatalytic activity of new (untested) structures at early stage of experimental design. The long-term goal is to create nano-QSPR models of TiO_2 based structures, to generate sufficient experimental and mechanistic data for experimental researchers that will help deciding which structural features should be used and/or changed in order to design novel and efficient

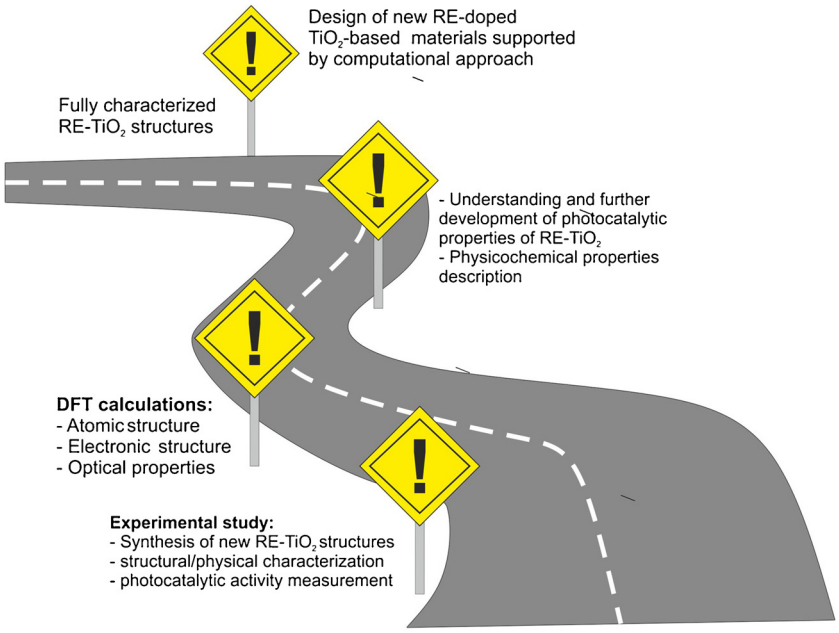

Fig. 9. Combined experimental and computational roadmap showing the objectives for first-principles calculations in supporting experimental procedures for the further design of new RE-TiO_2-based materials.

photocatalytic systems having desired properties (i.e. effective photocatalytic activity).

Acknowledgements

This research was financially supported by the Polish National Science Centre (grant No. NCN 2015/17/D/ST5/01331, 2014/15/N/ST5/02043, 2016/20/T/ST5/00280, 2015/19/N/NZ7/01593 and 2017/24/T/ST5/00221) and by the Foundation for Polish Science (FNP).

References

[1] R. Daghrir, P. Drogui, D. Robert, Modified TiO 2 for environmental photocatalytic applications: a review, Ind. Eng. Chem. Res. 52 (2013) 130226090752004, , http://dx.doi.org/10.1021/ie303468t.
[2] M.R.D. Khaki, M.S. Shafeeyan, A.A.A. Raman, W.M.A.W. Daud, Application of doped photocatalysts for organic pollutant degradation - a review, J. Environ. Manage. 198 (2017) 78–94, http://dx.doi.org/10.1016/j.jenvman.2017.04.099.
[3] J. Ma, M. Yang, Y. Sun, C. Li, Q. Li, F. Gao, F. Yu, J. Chen, Fabrication of Ag/TiO2 nanotube array with enhanced photo-catalytic degradation of aqueous organic pollutant, Phys. E Low-Dimension. Syst. Nanostruct. 58 (2014) 24–29, http://dx.doi.org/10.1016/j.physe.2013.11.006.
[4] M. Pelaez, N.T. Nolan, S.C. Pillai, M.K. Seery, P. Falaras, A.G. Kontos, P.S.M. Dunlop, J.W.J. Hamilton, J.A. Byrne, K.O. Shea, M.H. Entezari, D.D. Dionysiou, B. Applied Catalysis, Environmental a review on the visible light active titanium dioxide photocatalysts for environmental applications ☆, Appl. Catal. B Environ. 125 (2012) 331–349, http://dx.doi.org/10.1016/j.apcatb.2012.05.036.
[5] S. Rehman, R. Ullah, A.M. Butt, N.D. Gohar, Strategies of making TiO2 and ZnO visible light active, J. Hazard. Mater. 170 (2009) 560–569, http://dx.doi.org/10.1016/j.jhazmat.2009.05.064.
[6] S. Bingham, W.A. Daoud, Recent advances in making nano-sized TiO $_2$ visible-light active through rare-earth metal doping, J. Mater. Chem. 21 (2011) 2041–2050, http://dx.doi.org/10.1039/C0JM02271C.
[7] R. Asahi, T. Morikawa, H. Irie, T. Ohwaki, Nitrogen-Doped titanium dioxide as visible-light-sensitive photocatalyst: designs, developments, and prospects, Chem. Rev. 114 (2014) 9824–9852, http://dx.doi.org/10.1021/cr5000738.
[8] J. Reszczyńska, T. Grzyb, Z. Wei, M. Klein, E. Kowalska, B. Ohtani, A. Zaleska-Medynska, Photocatalytic activity and luminescence properties of RE3+–TiO2 nanocrystals prepared by sol–gel and hydrothermal methods, Appl. Catal. B Environ. 181 (2016) 825–837, http://dx.doi.org/10.1016/j.apcatb.2015.09.001.
[9] J. Reszczyńska, T. Grzyb, J.W. Sobczak, W. Lisowski, M. Gazda, B. Ohtani, A. Zaleska, Visible light activity of rare earth metal doped (Er3+, Yb3+ or Er3+/Yb3+) titania photocatalysts, Appl. Catal. B Environ. 163 (2015) 40–49, http://dx.doi.org/10.1016/j.apcatb.2014.07.010.
[10] P. Mazierski, W. Lisowski, T. Grzyb, M.J. Winiarski, T. Klimczuk, A. Mikołajczyk, J. Flisikowski, A. Hirsch, A. Kołakowska, T. Puzyn, A. Zaleska-Medynska, J. Nadolna, Enhanced photocatalytic properties of lanthanide-TiO2 nanotubes: an experimental and theoretical study, Appl. Catal. B Environ. 205 (2017) 376–385, http://dx.doi.org/10.1016/j.apcatb.2016.12.044.
[11] J. Reszczyńska, T. Grzyb, J.W. Sobczak, W. Lisowski, M. Gazda, B. Ohtani, A. Zaleska, Lanthanide co-doped TiO2: the effect of metal type and amount on surface properties and photocatalytic activity, Appl. Surf. Sci. 307 (2014) 333–345, http://dx.doi.org/10.1016/j.apsusc.2014.03.199.
[12] J. Reszczynska, D.A. Esteban, M. Gazda, A. Zaleska, Pr-DOPED TIO2. The effect of metal content on photocatalytic activity, Physiochem. Prob. Miner. Process. 50 (2014) 515–524.
[13] J. Reszczynska, A. Iwulska, G. Sliwinski, A. Zaleska, Characterization and photocatalytic activity of rare earth metal-doped titanium dioxide, Physiochem. Prob. Miner. Process. 48 (2012) 201–208.
[14] P. Mazierski, M. Nischk, M. Gołkowska, W. Lisowski, M. Gazda, M.J.M.J. Winiarski, T. Klimczuk, A. Zaleska-Medynska, Photocatalytic activity of nitrogen doped TiO2 nanotubes prepared by anodic oxidation: the effect of applied voltage, anodization time and amount of nitrogen dopant, Appl. Catal. B Environ. 196 (2016) 77–88, http://dx.doi.org/10.1016/j.apcatb.2016.05.006.
[15] A.S. Weber, A.M. Grady, R.T. Koodali, Lanthanide modified semiconductor photocatalysts, Catal. Sci. Technol. 2 (2012) 683, http://dx.doi.org/10.1039/c2cy00552b.
[16] M. Zalas, Gadolinium-modified titanium oxide materials for photoenergy applications: a review, J. Rare Earths 32 (2014) 487–495, http://dx.doi.org/10.1016/S1002-0721(14)60097-1.
[17] Y.U. Yaoguang, C. Gang, Z. Yansong, H.A.N. Zhonghui, Recent advances in rare-earth elements modification of inorganic semiconductor- based photocatalysts for efficient solar energy conversion : a review, J. Rare Earths 33 (2015) 453–462, http://dx.doi.org/10.1016/S1002-0721(14)60440-3.
[18] N. us Saqib, R. Adnan, I. Shah, A mini-review on rare earth metal-doped TiO2for photocatalytic remediation of wastewater, Environ. Sci. Pollut. Res. 23 (2016) 15941–15951, http://dx.doi.org/10.1007/s11356-016-6984-7.
[19] S. Bingham, Wa. Daoud, Recent advances in making nano-sized TiO2 visible-light active through rare-earth metal doping, J. Mater. Chem. 21 (2011) 2041, http://dx.doi.org/10.1039/c0jm02271c.
[20] W. Zhang, S. Yang, J. Li, W. Gao, Y. Deng, W. Dong, C. Zhao, G. Lu, Visible-to-ultraviolet upconvertion: energy transfer, material matrix, and synthesis strategies, Appl. Catal. B Environ. 206 (2017) 89–103, http://dx.doi.org/10.1016/j.apcatb.2017.01.023.
[21] M. Uzunova-Bujnova, R. Kralchevska, M. Milanova, R. Todorovska, D. Hristov, D. Todorovsky, Crystal structure, morphology and photocatalytic activity of modified TiO2 and of spray-deposited TiO2 films, Catal. Today 151 (2010) 14–20, http://dx.doi.org/10.1016/j.cattod.2010.02.058.
[22] H.S. Kibombo, A.S. Weber, C. Wu, K. Reddy, R.T. Koodali, Effectively dispersed europium oxide dopants in TiO2 aerogel supports for enhanced photocatalytic pollutant degradation, J. Photochem. Photobiol. A Chem. 269 (2013) 49–58, http://dx.doi.org/10.1016/j.jphotochem.2013.07.006.
[23] Y. Cao, Z. Zhao, J. Yi, C. Ma, D. Zhou, R. Wang, C. Li, J. Qiu, Luminescence properties of Sm3+-doped TiO2 nanoparticles : synthesis, characterization, and mechanism, J. Alloys Compd. 554 (2013) 12–20, http://dx.doi.org/10.1016/j.jallcom.2012.11.149.
[24] L. Yu, X. Yang, J. He, Y. He, D. Wang, One-step hydrothermal method to prepare

nitrogen and lanthanum co-doped TiO 2 nanocrystals with exposed {0 0 1} facets and study on their photocatalytic activities in visible light, J. Alloy Compd. 637 (2015) 308–314, http://dx.doi.org/10.1016/j.jallcom.2015.03.035.
[25] J. Wang, F.Y. Wen, Z.H. Zhang, X.D. Zhang, Z.J. Pan, P. Zhang, P.L. Kang, J. Tong, L. Wang, L. Xu, Investigation on degradation of dyestuff wastewater using visible light in the presence of a novel nano TiO2 catalyst doped with upconversion luminescence agent, J. Photochem. Photobiol. A Chem. 180 (2006) 189–195, http://dx.doi.org/10.1016/j.jphotochem.2005.10.016.
[26] O.A. Goryacheva, N.V. Beloglazova, A.M. Vostrikova, M.V. Pozharov, A.M. Sobolev, I.Y. Goryacheva, Lanthanide-to-quantum dot Forster resonance energy transfer (FRET): application for immunoassay, Talanta 164 (2017) 377–385, http://dx.doi.org/10.1016/j.talanta.2016.11.054.
[27] W. Zhan, Y. Guo, X. Gong, Y. Guo, Y. Wang, G. Lu, Current status and perspectives of rare earth catalytic materials and catalysis, Chin. J. Catal. 35 (2014) 1238–1250, http://dx.doi.org/10.1016/S1872-2067(14)60189-3.
[28] A. Bahtat, M. Bouazaoui, M. Bahtat, C. Garapon, B. Jacquier, J. Mugnier, Up-conversion fluorescence spectroscopy in Er3+: TiO2 planar waveguides prepared by a sol-gel process, J. Non Cryst. Solids 202 (1996) 16–22, http://dx.doi.org/10.1016/0022-3093(96)00172-X.
[29] K.L. Frindell, M.H. Bartl, M.R. Robinson, G.C. Bazan, A. Popitsch, G.D. Stucky, Visible and near-IR luminescence via energy transfer in rare earth doped mesoporous titania thin films with nanocrystalline walls, J. Solid State Chem. 172 (2003) 81–88, http://dx.doi.org/10.1016/S0022-4596(02)00126-3.
[30] L. Liang, Y. Yulin, Z. Mi, F. Ruiqing, Q. LeLe, W. Xin, Z. Lingyun, Z. Xuesong, H. Jianglong, Enhanced performance of dye-sensitized solar cells based on TiO2 with NIR-absorption and visible upconversion luminescence, J. Solid State Chem. 198 (2013) 459–465, http://dx.doi.org/10.1016/j.jssc.2012.10.013.
[31] J. Castañeda-Contreras, V.F. Marañón-Ruiz, R. Chiu-Zárate, H. Pérez-Ladrón de Guevara, R. Rodriguez, C. Michel-Uribe, Photocatalytic activity of erbium-doped TiO2 nanoparticles immobilized in macro-porous silica films, Mater. Res. Bull. 47 (2012) 290–295, http://dx.doi.org/10.1016/j.materresbull.2011.11.021.
[32] M. Borlaf, S. Caes, J. Dewalque, M.T. Colomer, R. Moreno, R. Cloots, F. Boschini, Effect of the RE (RE = Eu, Er) doping on the structural and textural properties of mesoporous TiO2 thin films obtained by evaporation induced self-assembly method, Thin Solid Films 558 (2014) 140–148, http://dx.doi.org/10.1016/j.tsf.2014.03.002.
[33] C.-H. Liang, M.-F. Hou, S.-G. Zhou, F.-B. Li, C.-S. Liu, T.-X. Liu, Y.-X. Gao, X.-G. Wang, J.-L. Lü, The effect of erbium on the adsorption and photodegradation of orange I in aqueous Er3+-TiO2 suspension, J. Hazard. Mater. 138 (2006) 471–478, http://dx.doi.org/10.1016/j.jhazmat.2006.05.066.
[34] S. Obregón, a. Kubacka, M. Fernández-García, G. Colón, High-performance Er3+–TiO2 system: dual up-conversion and electronic role of the lanthanide, J. Catal. 299 (2013) 298–306, http://dx.doi.org/10.1016/j.jcat.2012.12.021.
[35] R. Salhi, J.-L.L. Deschanvres, Efficient green and red up-conversion emissions in Er/Yb co-doped TiO2 nanopowders prepared by hydrothermal-assisted sol-gel process, J. Lumin. 176 (2016) 250–259, http://dx.doi.org/10.1016/j.jlumin.2016.03.011.
[36] X. Mao, B. Yan, J. Wang, J. Shen, Up-conversion fluorescence characteristics and mechanism of Er3+-doped TiO2 thin films, Vacuum 102 (2014) 38–42, http://dx.doi.org/10.1016/j.vacuum.2013.10.026.
[37] D.Y. Lee, J.-T. Kim, J.-H. Park, Y.-H. Kim, I.-K. Lee, M.-H. Lee, B.-Y. Kim, Effect of Er doping on optical band gap energy of TiO2 thin films prepared by spin coating, Curr. Appl. Phys. (2013) 1–5, http://dx.doi.org/10.1016/j.cap.2013.03.025.
[38] C.-L.L. Jia, Z.-N.N. Wei, R. Zhou, Structural properties of rutile TiO2 bombarded with Er ions, Nucl. Instrum. Methods Phys. Res. Sect. B Beam Interact. Mater. Atoms 313 (2013) 50–53, http://dx.doi.org/10.1016/j.nimb.2013.08.026.
[39] Y. Li, Y. Wang, J. Kong, J. Wang, Synthesis and photocatalytic activity of TiO2 nanotubes co-doped by erbium ions, Appl. Surf. Sci. 328 (2015) 115–119, http://dx.doi.org/10.1016/j.apsusc.2014.12.054.
[40] J.-G. Li, X.-H. Wang, H. Kamiyama, T. Ishigaki, T. Sekiguchi, RF plasma processing of Er-doped TiO2 luminescent nanoparticles, Thin Solid Films 506–507 (2006) 292–296, http://dx.doi.org/10.1016/j.tsf.2005.08.093.
[41] S. Obregon, G. Colon, Evidence of upconversion luminescence contribution to the improved photoactivity of erbium doped TiO2 systems, Chem. Commun. 48 (2012) 7865–7867, http://dx.doi.org/10.1039/C2CC33391K.
[42] Y. Yang, C. Zhang, Y. Xu, H. Wang, X. Li, C. Wang, Electrospun Er: TiO2 nanofibrous films as efficient photocatalysts under solar simulated light, Mater. Lett. 64 (2010) 147–150, http://dx.doi.org/10.1016/j.matlet.2009.10.028.
[43] T. Ji, Y. Liu, H. Zhao, H. Du, J. Sun, G. Ge, Preparation and up-conversion fluorescence of rare earth (Er3+ or Yb3+/Er3+)-doped TiO2 nanobelts, J. Solid State Chem. 183 (2010) 584–589, http://dx.doi.org/10.1016/j.jssc.2010.01.004.
[44] D. Falcomer, M. Daldosso, C. Cannas, A. Musinu, B. Lasio, S. Enzo, A. Speghini, M. Bettinelli, A one-step solvothermal route for the synthesis of nanocrystalline anatase TiO2 doped with lanthanide ions, J. Solid State Chem. 179 (2006) 2452–2457, http://dx.doi.org/10.1016/j.jssc.2006.04.043.
[45] A. Bahtat, M. Bouazaoui, M. Bahtat, C. Garapon, B. Jacquier, J. Mugnier, Up-conversion fluorescence spectroscopy in ce{Er^3+}: ce{TiO2} planar waveguides prepared by a sol-gel process, J. Non-Cryst Solids 202 (1996) 16–22, http://dx.doi.org/10.1016/0022-3093(96)00172-X.
[46] Y. Zheng, W. Wang, Electrospun nanofibers of Er3+-doped TiO2 with photocatalytic activity beyond the absorption edge, J. Solid State Chem. 210 (2014) 206–212, http://dx.doi.org/10.1016/j.jssc.2013.11.029.
[47] H. Wang, Y. Wang, Y. Yang, X. Li, C. Wang, Photoluminescence properties of the rare-earth ions in the TiO2 host nanofibers prepared via electrospinning, Mater. Res. Bull. 44 (2009) 408–414, http://dx.doi.org/10.1016/j.materresbull.2008.05.001.
[48] S. Obregon, G. Colon, S. Obregón, G. Colón, Evidence of upconversion luminescence contribution to the improved photoactivity of erbium doped TiO2 systems, Chem. Commun. 48 (2012) 7865, http://dx.doi.org/10.1039/C2CC33391K.
[49] V.C. Bhethanabotla, D.R. Russell, J.N. Kuhn, Assessment of mechanisms for enhanced performance of Yb/Er/titania photocatalysts for organic degradation: role of rare earth elements in the titania phase, Appl. Catal. B Environ. 202 (2017) 156–164, http://dx.doi.org/10.1016/j.apcatb.2016.09.008.
[50] J.W. Pickering, V.R. Bhethanabotla, J.N. Kuhn, Assessment of mechanisms for enhanced performance of TiO2/YAG:Yb+3,Er+3 composite photocatalysts for organic degradation, Appl. Catal. B Environ. 202 (2017) 147–155, http://dx.doi.org/10.1016/j.apcatb.2016.09.007.
[51] D. Hou, R. Goei, X. Wang, P. Wang, T.-T. Lim, Preparation of carbon-sensitized and Fe–Er codoped TiO2 with response surface methodology for bisphenol a photocatalytic degradation under visible-light irradiation, Appl. Catal. B Environ. 126 (2012) 121–133, http://dx.doi.org/10.1016/j.apcatb.2012.07.012.
[52] Q. Shang, H. Yu, X. Kong, H. Wang, X. Wang, Y. Sun, Green and red up-conversion emissions of Er 3 + – Yb 3 + Co-doped TiO 2 nanocrystals prepared by sol – gel method, J. Lumin. 128 (2008) 1211–1216, http://dx.doi.org/10.1016/j.jlumin.2007.11.097.
[53] S.P. Sahu, S.L. Cates, H.-I. Kim, J.-H. Kim, E.L. Cates, The myth of visible light photocatalysis using lanthanide upconversion materials, Environ. Sci. Technol. 52 (2018) 2973–2980, http://dx.doi.org/10.1021/acs.est.7b05941.
[54] H. Cai, G. Liu, W. Lü, X. Li, L. Yu, D. Li, Effect of Ho-doping on photocatalytic activity of nanosized TiO2 catalyst, J. Rare Earths 26 (2008) 71–75, http://dx.doi.org/10.1016/S1002-0721(08)60040-X.
[55] J.-W. Shi, J.-T. Zheng, P. Wu, Preparation, characterization and photocatalytic activities of holmium-doped titanium dioxide nanoparticles, J. Hazard. Mater. 161 (2009) 416–422, http://dx.doi.org/10.1016/j.jhazmat.2008.03.114.
[56] W. Zhou, Y. He, Ho/TiO2 nanowires heterogeneous catalyst with enhanced p hotocatalytic properties by hydrothermal synthesis met hod, Chem. Eng. J. 179 (2012) 412–416, http://dx.doi.org/10.1016/j.cej.2011.10.094.
[57] J.-W. Shi, J.-T. Zheng, Y. Hu, Y.-C. Zhao, Influence of Fe3+ and Ho3+ co-doping on the photocatalytic activity of TiO2, Mater. Chem. Phys. 106 (2007) 247–249, http://dx.doi.org/10.1016/j.matchemphys.2007.05.042.
[58] D. Dorosz, J. Zmojda, M. Kochanowicz, P. Miluski, P. Jelen, M. Sitarz, Structural and optical study on antimony-silicate glasses doped with thulium ions, Spectrochim. Acta Part A Mol. Biomol. Spectrosc. 134 (2015) 608–613, http://dx.doi.org/10.1016/j.saa.2014.06.070.
[59] R. Lauro, J. Ruggiero, A. Louchet, A. Alexander, T. Chanelière, I. Lorgeré, F. Bretenaker, F. Goldfarb, J.L. Le Gouët, Thulium doped crystals for quantum information storage, J. Lumin. 129 (2009) 1951–1954, http://dx.doi.org/10.1016/j.jlumin.2009.03.025.
[60] Ma. Lourenço, C. Opoku, R.M. Gwilliam, K.P. Homewood, Photoluminescence study of thulium-doped silicon substrates for light emitting diodes, Opt. Mater. (Amst. 32 (2010) 1597–1600, http://dx.doi.org/10.1016/j.optmat.2010.05.026.
[61] W. Ryba-Romanowski, R. Lisiecki, H. Jelinková, J. Šulc, Thulium-doped vanadate crystals: growth, spectroscopy and laser performance, J. Prog. Quantum Electron. 35 (2011) 109–157, http://dx.doi.org/10.1016/j.pquantelec.2011.06.001.
[62] J. Navas, A. Sánchez-Coronilla, T. Aguilar, D.M. De los Santos, N.C. Hernández, R. Alcántara, C. Fernández-Lorenzo, J. Martín-Calleja, Thermo-selective Tm $_x$ Ti $_{1-x}$ O $_{2-x/2}$ nanoparticles: from Tm-doped anatase TiO $_2$ to a rutile/pyrochlore Tm $_2$ Ti $_2$ O $_7$ mixture. An experimental and theoretical study with a photoca, Nanoscale 6 (2014) 12740–12757, http://dx.doi.org/10.1039/C4NR03715D.
[63] D.M. de los Santos, J. Navas, T. Aguilar, A. Sánchez-Coronilla, R. Alcántara, C. Fernández-Lorenzo, G. Blanco, J.M. Calleja, Study of thulium doping effect and enhancement of photocatalytic activity of rutile TiO2 nanoparticles, Mater. Chem. Phys. 161 (2015) 175–184, http://dx.doi.org/10.1016/j.matchemphys.2015.05.034.
[64] D.M. de los Santos, J. Navas, T. Aguilar, A. Sanchez-Coronilla, C. Fernandez-Lorenzo, R. Alcantara, J.C. Pinero, G. Blanco, J. Martin-Calleja, Tm-doped TiO2 and Tm2Ti2O7 pyrochlore nanoparticles: enhancing the photocatalytic activity of rutile with a pyrochlore phase, Beilstein J. Nanotechnol. 6 (2015) 605–616, http://dx.doi.org/10.3762/bjnano.6.62.
[65] A.V. Shlyakhtina, L.G. Shcherbakova, A.V. Knotko, A.V. Steblevskii, Study of the Fluorite?Pyrochlore?Fluorite phase transitions in Ln2Ti2O7 (Ln = Lu, Yb, Tm), J. Solid State Electrochem. 8 (2004) 661–667, http://dx.doi.org/10.1007/s10008-003-0491-8.
[66] A. Bokare, M. Pai, A.A. Athawale, Surface modified Nd doped TiO 2 nanoparticles as photocatalysts in UV and solar light irradiation, Sol. Energy 91 (2013) 111–119, http://dx.doi.org/10.1016/j.solener.2013.02.005.
[67] T.L.R. Hewer, E.C.C. Souza, T.S. Martins, E.N.S. Muccillo, R.S. Freire, Influence of neodymium ions on photocatalytic activity of TiO2 synthesized by sol-gel and precipitation methods, J. Mol. Catal. A Chem. 336 (2011) 58–63, http://dx.doi.org/10.1016/j.molcata.2010.12.010.
[68] Z.M. El-Bahy, A.A. Ismail, R.M. Mohamed, Enhancement of titania by doping rare earth for photodegradation of organic dye (direct Blue), J. Hazard. Mater. 166 (2009) 138–143, http://dx.doi.org/10.1016/j.jhazmat.2008.11.022.
[69] J. Du, H. Chen, H. Yang, R. Sang, Y. Qian, Y. Li, G. Zhu, Y. Mao, W. He, D.J. Kang, A facile sol-gel method for synthesis of porous Nd-doped TiO2 monolith with enhanced photocatalytic activity under uv-vis irradiation, Microporous Mesoporous Mater. 182 (2013) 87–94, http://dx.doi.org/10.1016/j.micromeso.2013.08.023.
[70] F.B. Li, K.H. Ng, X.Z. Li, K.H. Ng, Photocatalytic degradation of an odorous pollutant: 2-Mercaptobenzothiazole in aqueous suspension using Nd3+—TiO2 catalysts, Ind. Eng. Chem. Res. 45 (2006) 1–7, http://dx.doi.org/10.1021/ie050139o.
[71] D. Wojcieszak, M. Mazur, M. Kurnatowska, D. Kaczmarek, J. Domaradzki, L. Kepinski, K. Chojnacki, Influence of Nd-Doping on photocatalytic properties of TiO 2 nanoparticles and thin film coatings, Int. J. Photoenergy 2014 (2014), http://

dx.doi.org/10.1155/2014/463034.
[72] R. Kralchevska, M. Milanova, D. Hristov, A. Pintar, D. Todorovsky, Synthesis, characterization and photocatalytic activity of neodymium, nitrogen and neodymium-nitrogen doped TiO 2, Mater. Res. Bull. 47 (2012) 2165–2177, http://dx.doi.org/10.1016/j.materresbull.2012.06.009.
[73] F.B. Li, X.Z. Li, K.W. Cheah, Photocatalytic activity of neodymium ion doped TiO2 for 2-Mercaptobenzothiazole degradation under visible light irradiation, Environ. Chem. 2 (2005) 130–137, http://dx.doi.org/10.1071/EN05008.
[74] S. Rengaraj, S. Venkataraj, J.W. Yeon, Y. Kim, X.Z. Li, G.K.H. Pang, Preparation, characterization and application of Nd-TiO2 photocatalyst for the reduction of Cr (VI) under UV light illumination, Appl. Catal. B Environ. 77 (2007) 157–165, http://dx.doi.org/10.1016/j.apcatb.2007.07.016.
[75] Y.-H. Xu, C. Chen, X.-L. Yang, X. Li, B.-F. Wang, Preparation, characterization and photocatalytic activity of the neodymium-doped TiO2 nanotubes, Appl. Surf. Sci. 255 (2009) 8624–8628, http://dx.doi.org/10.1016/j.apsusc.2009.06.036.
[76] D. Nassoko, Y.F. Li, J.L. Li, X. Li, Y. Yu, Neodymium-doped TiO 2 with anatase and brookite two phases: mechanism for photocatalytic activity enhancement under visible light and the role of electron, Int. J. Photoenergy 2012 (2012), http://dx.doi.org/10.1155/2012/716087.
[77] V. Gomez, A.M. Balu, J.C. Serrano-Ruiz, S. Irusta, D.D. Dionysiou, R. Luque, J. Santamaría, Microwave-assisted mild-temperature preparation of neodymium-doped titania for the improved photodegradation of water contaminants, Appl. Catal. A Gen. 441–442 (2012) 47–53, http://dx.doi.org/10.1016/j.apcata.2012.07.003.
[78] C. Wang, Y. Ao, P. Wang, J. Hou, J. Qian, Preparation, characterization and photocatalytic activity of the neodymium-doped TiO2 hollow spheres, Appl. Surf. Sci. 257 (2010) 227–231, http://dx.doi.org/10.1016/j.apsusc.2010.06.071.
[79] Y. Xie, C. Yuan, Photocatalysis of neodymium ion modified TiO2 sol under visible light irradiation, Appl. Surf. Sci. 221 (2004) 17–24, http://dx.doi.org/10.1016/S0169-4332(03)00945-0.
[80] P. Parnicka, P. Mazierski, T. Grzyb, Z. Wei, E. Kowalska, B. Ohtani, W. Lisowski, T. Klimczuk, J. Nadolna, Preparation and photocatalytic activity of Nd-modified TiO2 photocatalysts: insight into the excitation mechanism under visible light, J. Catal. 353 (2017) 211–222, http://dx.doi.org/10.1016/j.jcat.2017.07.017.
[81] N.R. Khalid, E. Ahmed, Z. Hong, Y. Zhang, M. Ullah, M. Ahmed, Graphene modified Nd/TiO2 photocatalyst for methyl orange degradation under visible light irradiation, Ceram. Int. 39 (2013) 3569–3575, http://dx.doi.org/10.1016/j.ceramint.2012.10.183.
[82] P. Parnicka, P. Mazierski, T. Grzyb, W. Lisowski, E. Kowalska, B. Ohtani, A. Zaleska-Medynska, J. Nadolna, Influence of the preparation method on the photocatalytic activity of Nd-modified TiO2, Beilstein J. Nanotechnol. 9 (2018) 447–459, http://dx.doi.org/10.3762/bjnano.9.43.
[83] S. Lutfalla, V. Shapovalov, A.T. Bell, Calibration of the DFT/GGA + U method for determination of reduction energies for transition and rare earth metal oxides of Ti, V, Mo, and Ce, J. Chem. Theory Comput. 7 (2011) 2218–2223, http://dx.doi.org/10.1021/ct200202g.
[84] Z.-N. Wei, C.-L. Jia, First-principle calculations of the electronic and optical properties of Tm-doped anatase titanium dioxide, Opt. Eng. 54 (2015) 37107, http://dx.doi.org/10.1117/1.OE.54.3.037107.
[85] E. Bruyer, A. Sayede, Density functional calculations of the structural, electronic, and ferroelectric properties of high-k titanate Re2Ti2O7 (Re = La and Nd), J. Appl. Phys. 108 (2010) 53705, http://dx.doi.org/10.1063/1.3459891.
[86] D.W. Hwang, J.S. Lee, W. Li, S.H. Oh, Electronic band structure and photocatalytic activity of Ln $_2$ Ti $_2$ O $_7$ (Ln = La, Pr, Nd), J. Phys. Chem. B 107 (2003) 4963–4970, http://dx.doi.org/10.1021/jp034229n.
[87] W. Li, Y. Wang, H. Lin, S.I. Shah, C.P. Huang, D.J. Doren, S.A. Rykov, J.G. Chen, M.A. Barteau, Band gap tailoring of Nd3 + -doped TiO2 nanoparticles, Appl. Phys. Lett. 83 (2003) 4143–4145, http://dx.doi.org/10.1063/1.1627962.
[88] G. Kresse, D. Joubert, From ultrasoft pseudopotentials to the projector augmented-wave method, Phys. Rev. B 59 (1999) 1758–1775, http://dx.doi.org/10.1103/PhysRevB.59.1758.
[89] G. Kresse, J. Furthmüller, Efficiency of ab-initio total energy calculations for metals and semiconductors using a plane-wave basis set, Comput. Mater. Sci. 6 (1996) 15–50, http://dx.doi.org/10.1016/0927-0256(96)00008-0.
[90] Y. Zhang, W. Lin, Y. Li, K. Ding, J. Li, A theoretical study on the electronic structures of TiO2: effect of hartre fock Exchange, J. Phys. Chem. B 109 (2005) 19270–19277, http://dx.doi.org/10.1021/jp0523625.
[91] C. Di Valentin, G. Pacchioni, A. Selloni, Electronic structure of defect states in hydroxylated and reduced rutile TiO2(110) surfaces, Phys. Rev. Lett. 97 (2006), http://dx.doi.org/10.1103/PhysRevLett.97.166803.
[92] R. Balda, J. Fernández, E.E. Nyein, U. Hömmerich, Infrared to visible upconversion of Nd 3 + ions in KPb 2 Br 5 low phonon crystal, Opt. Express 14 (2006) 3993–4004, http://dx.doi.org/10.1364/OE.14.003993.
[93] P.V. Ramakrishna, S.V.N. Pammi, K. Samatha, UV–visible upconversion studies of Nd3 + ions in lead tellurite glass, Solid State Commun. 155 (2013) 21–24, http://dx.doi.org/10.1016/j.ssc.2012.10.043.
[94] J.-C.G. Bünzli, C. Piguet, Taking advantage of luminescent lanthanide ions, Chem. Soc. Rev. 34 (2005) 1048, http://dx.doi.org/10.1039/b406082m.
[95] J.C.G. B??nzli, Lanthanide light for biology and medical diagnosis, J. Lumin. 170 (2016) 866–878, http://dx.doi.org/10.1016/j.jlumin.2015.07.033.
[96] A. Mikolajczyk, A. Malankowska, G. Nowaczyk, A. Gajewicz, S. Hirano, S. Jurga, A. Zaleska-Medynska, T. Puzyn, Combined experimental and computational approach to developing efficient photocatalysts based on Au/Pd-TiO2 nanoparticles, Environ. Sci. Nano 3 (2016) 1425–1435, http://dx.doi.org/10.1039/C6EN00232C.
[97] A. Krukowska, M.J. Winiarski, J. Strychalska-Nowak, T. Klimczuk, W. Lisowski, A. Mikolajczyk, H.P. Pinto, T. Puzyn, T. Grzyb, A. Zaleska-Medynska, Rare earth ions doped K2Ta2O6 photocatalysts with enhanced UV–vis light activity, Appl. Catal. B Environ. 224 (2018) 451–468, http://dx.doi.org/10.1016/j.apcatb.2017.10.061.
[98] A. Mikolajczyk, H.P. Pinto, A. Gajewicz, T. Puzyn, J. Leszczynski, *Ab Initio* studies of anatase TiO_2 (101) surface-supported Au_8 clusters, Curr. Top. Med. Chem. 15 (2015) 1859–1867, http://dx.doi.org/10.2174/1568026615666150506151826.